

TEMPERATURE CONTROLS ON NO-ANALOG COMMUNITY ESTABLISHMENT IN
THE GREAT LAKES REGION

by

David Fastovich

A thesis submitted in partial fulfillment of
requirements for the degree of

Master of Science

(Geography)

at the

UNIVERSITY OF WISCONSIN - MADISON

2018

Abstract

Temperature reconstructions in eastern North America from pollen are rife in the literature, but these reconstructions cannot be used to study the sensitivity and response time of vegetation to temperature changes. Branched glycerol dialkyl glycerol tetraethers (brGDGT) have recently been applied to reconstruct temperature at Silver Lake, OH, where the resulting temperature estimates closely tracked a regional pollen temperature reconstruction for the southern Great Lakes region. Here, we present the second brGDGT temperature record in this region, at Bonnet Lake, OH, using a new method for brGDGT detection and four alternative calibration functions, and reanalyze sediments from Silver Lake. We compare results across brGDGT detection methods, between sites and among calibration functions, and assess calibration uncertainty using a Bayesian linear regression.

Of the calibration functions, MAT MBT'_{5Me} reproduced the regional pollen stack and existing temperature record from Silver Lake most closely but is ~2°C warmer on average than the existing brGDGT temperature record. In the Bayesian regression analyses, the 95% credible interval when using the calibration from Weijers et al. (2007) was +/- 12.3°C. The MAT MBT'_{5Me} calibration from De Jonge et al. (2014) had a smaller uncertainty (+/- 9.8°C 95% credible interval), likely resulting from a reduced sensitivity of brGDGT methylation to pH. These uncertainties are based only on analyses of the calibration data and likely overestimate reconstruction uncertainty, because calibration soil samples are heterogenous at the sampling scale and are at locations distant from the corresponding temperature measurement. Uncertainty can be reduced by creating improved calibration datasets of modern lake sediments. Despite uncertainty in absolute temperature and range, climatic trends are closely similar among brGDGT reconstructions and provide insight into the temperature drivers of past vegetation dynamics. *Picea* decline begins shortly after the start of Bølling-Allerød warming. The establishment and disappearance of no-analog communities lag temperature change by 200-500 years at Bonnet Lake and Silver Lake. The lack of synchrony in the timing of warming and no-analog community establishment at Bonnet Lake and Silver Lake, but agreement in the sequence of events, indicates that local climate is an important control on vegetation assemblages. The extension of brGDGTs to the Great Lakes Region is further supported in this study, but uncertainty in temperature estimates emphasizes the need for improved calibration datasets.

Acknowledgments

This thesis would have never been possible without the help of incredible people. I want to first thank Doug and Jamille Hawkins, the landowners of the Long Lake Park Campground, who graciously let us take sediment cores from their lake to better understand the vegetation history of the region. Tom Lowell and Greg Wiles helped immensely by recommending Bonnet as a promising site and sharing experience based on prior visits. The National Science Foundation funded this research (award: DEB-1353896).

I'm indebted to the team of people (Jack Williams, Ben Bates, Kevin Burke, Yue Wang, Tom Lowell, Jackie Rodriguez) who retrieved the cores that I analyzed – without them I would have had nothing to do these past two years! Kate Hayes, Joe Bevington, and Bailey Zak are undergraduate assistants who were instrumental in helping prepare the data presented here, their long hours in the lab are greatly appreciated. Ben Watson (UW-Madison MSc 2017) was an incredible resource during my transition into the Williams Lab, and despite him having job responsibilities of his own a few thousand miles away, he never hesitated to answer any questions I had. I owe many thanks to Jim Russell for opening his lab to me and allowing me to learn a little bit about the world of organic geochemistry. Yue Wang spent countless hours with me in the lab teaching me the ins and outs of palynology. Much of the statistical analysis performed here would not have been possible without Mathias Trachsel who took time to not only help me with the analysis but made sure I understood the concepts behind the statistics. To my friends in the Williams Lab, thank you for welcoming me and making Madison such a great place to live. I owe a great amount of gratitude to my committee members Monica Turner and Joe Mason for devoting much of their little free time to helping improve my research. I can't thank my advisor, Jack Williams, enough for providing me with an opportunity to continue the work he started. Your mentorship and unending patience will have a lasting impact on my personal and professional life to follow.

Lastly, I want to thank Lydia - this would have been impossible without your endless support and love. Your constant encouragement kept me going and I can't wait to repay the support.

Table of Contents

Introduction	1
Research Questions and Hypotheses	5
Background and Literature Review	8
<i>Deglacial Climate History: Last Glacial Maximum to Early Holocene</i>	8
<i>Vegetation History of the Great Lakes Region</i>	12
<i>brGDGT as a Paleotemperature Proxy</i>	16
Study Site	19
Methods	19
<i>Core Collection</i>	19
<i>Geochronology</i>	20
<i>Loss-on-Ignition</i>	22
<i>Pollen Analysis</i>	23
<i>Dissimilarity Analysis</i>	25
<i>brGDGT Processing and Analysis</i>	26
<i>brGDGT Temperature Reconstruction</i>	27
Results	29
<i>Geochronology</i>	29
<i>Loss-on-Ignition</i>	29
<i>Vegetation History</i>	30
<i>brGDGT Temperature Reconstruction</i>	32
Discussion	35
<i>brGDGT Temperature Reconstructions</i>	35
<i>Temperature Controls on Late-Quaternary Vegetation Dynamics</i>	40
Conclusion	43
References	45
Tables	58
Figures	61
Appendix I. Supplemental Figures	69
Appendix II. Bonnet Lake Pollen Counts	71

Introduction

Plant communities composed of mesic broadleaf taxa and coniferous taxa were an important feature of the Great Lakes region during deglaciation (Cushing 1965, Gonzales et al. 2009, Jackson and Williams 2004, Overpeck et al. 1992, Williams and Jackson 2007, Williams et al. 2001). Unlike modern mixed forests, these communities were composed of taxa (*Picea*, *Fraxinus*, *Ulmus*, *Ostrya/Carpinus*, *Ambrosia*) that today only co-occur at low abundances (Jackson and Overpeck 2000). The presence of no-analog communities has been of interest to biogeographers studying species and community responses to a changing climate. Although early hypotheses posited that these communities formed by disequilibrium processes, their long duration now suggests that they formed in response to environmental conditions also without modern analog, but the relative importance of abiotic and biotic factors remains unclear. Changing seasonality of insolation and temperature resulting from different-than-present orbital parameters (Williams and Jackson 2007), rising temperature (Kutzbach et al. 1998), and megaherbivory release (Gill et al. 2012, Gill et al. 2009) all may have influenced the creation of no-analog communities. Temperature change and megaherbivory release are likely highly important in controlling local establishment of no-analog communities, yet demonstrating their effect remains challenged by a scarcity of independent proxies for these variables.

Testing the importance of temperature as a driver in deglacial vegetation dynamics and the length of time lags between temperature forcing and vegetation response has been limited by a scarcity of independent temperature proxies in lake sedimentary cores (Powers et al. 2004). Pollen transfer functions have been widely used to reconstruct past temperature variations (e.g. Bartlein et al. 2011, Marlon et al. 2017, Marsicek et al. 2018, Viau et al. 2012, Webb et al. 2003). These multivariate transfer functions are able to statistically deconvolve and reconstruct

the multiple climatic factors that control species distribution and population abundances, thereby generating paleoclimatic reconstructions from fossil pollen assemblages (Birks 1995, Imbrie and Webb 1981). However, these approaches generally are not able to assess the role of non-climatic controls on deglacial vegetation dynamics, such as the hypothesis that megafaunal extinction influenced broadleaf taxa expansion. Additionally, due to concerns of circularity, these approaches cannot be used to study the effect of climate on past vegetation dynamics.

While limited, independent proxies have been used to determine climatic changes in eastern North America. Stable isotopes from bulk marl and mollusks shells in lake sediments have proven useful in comparing climatic changes in the interior of continents with those from Greenland and Antarctica (Hu et al. 1997, Yu 2007, Yu and Eicher 1998, Yu 2000). However, multiple controls on the fractionation of stable isotopes in authigenic carbonates limit the ability to quantitatively estimate temperature (Hu et al. 1997, Leng and Marshall 2004). Stable isotopes have also been used as a climatic proxy in subfossil wood (Voelker et al. 2015). Voelker et al. (2015) were able to estimate summer precipitation using two stable isotopes $\delta^{18}\text{O}$ and δD from tree rings of subfossil wood retrieved from fluvial sediments in Missouri and adjacent regions. This method required the use of a mechanistic model of isotope fractionation and relied in part on pollen-based temperature reconstructions from Gonzales et al. (2009), so its inferences are not fully independent of the pollen data. In addition to stable isotopes, these fossil samples have been used for quantitative temperature estimates based on the size of earlywood and cambial age in tree rings (Voelker et al. 2012). This approach required a modern calibration of tree ring characteristics to temperature measurements from meteorological stations which produced a transfer function that was then applied to tree rings from subfossil wood (Voelker et al. 2012). Although such records are valuable, the scarcity of sufficiently old subfossil wood precludes the

wide use of this approach and the resulting temperature record can contain large gaps (Voelker et al. 2012). The current independent paleoclimatic proxies can reconstruct various elements of past climate states, but each has limitations.

Glycerol dialkyl glycerol tetraethers (GDGTs) are a group of bacterial and archaeal membrane lipids that have been applied in both marine and lacustrine environments to reconstruct mean surface temperatures (Loomis et al. 2015, Schouten et al. 2002). Their paleoclimatic application in lacustrine environments has ranged across a variety of climates and regions (Loomis et al. 2015, Sun et al. 2011, Zink et al. 2010). The temperature reconstruction relies upon calibration equations that are based on contemporary spatial datasets, consisting of GDGT measurements, mostly from soil samples, and associated temperatures from meteorological stations (Peterse et al. 2012, Sun et al. 2011, Weijers et al. 2007), with various calibration functions proposed. Lake sediment calibrations have also been produced for parts of Africa, offering more accurate temperature reconstructions than those based on soil datasets (Loomis et al. 2012, Loomis et al. 2015). Calibration datasets remain sparse, particularly in the Americas, and the choice of best calibration function remains uncertain for eastern North America.

Watson et al. (2018) developed a new brGDGT record for Silver Lake, Ohio (the first reported in eastern North America) and compared two brGDGT temperature reconstructions using calibrations from Weijers et al. (2007) and Peterse et al. (2012) to each other and to site-level and regional pollen-based temperature reconstruction. Good agreement between the brGDGT temperature reconstruction with the regional pollen-based temperature reconstructions supported the use of brGDGTs to infer past temperatures in eastern North America. The reconstructed temperature lagged Northern Hemispheric temperature change for the Bølling-

Allerød and Younger Dryas by ~300 yrs (Shakun et al. 2012, Watson et al. 2018). The cause of this lag is uncertain and may indicate a regional lag mediated by regional responses to ice sheet controls on climate (Watson et al. 2018). However, because this GDGT record is just for a single site, more work is needed to examine the regional changes in temperature by testing the reproducibility of reconstructed temperatures at multiple sites. Additionally, Watson et al. (2018) relied on an older method that does not discriminate some isomers of individual brGDGTs. Newer methods have been developed that enable finer molecular resolution and thereby more accurate calibrations (De Jonge et al. 2013, De Jonge et al. 2014, Hopmans et al. 2016). In addition, while the importance of measurement error has been assessed in prior work involving brGDGTs (Naafs et al. 2017), uncertainty in the calibration of the GDGT-temperature relationship has not.

In this study, I present a new multiproxy record from Bonnet Lake, Ohio comprising fossil pollen data, loss-on-ignition, and brGDGT-inferred temperature. Uncertainty in the temperature reconstruction is quantified by comparing an ensemble of temperature reconstructions. The ensemble of temperature reconstructions is produced by generating a distribution of calibration parameters using data from De Jonge et al. (2014) and Weijers et al. (2007) and applying a Bayesian linear model instead of an ordinary least squares linear model. Use of the Bayesian linear model enables estimates of calibration uncertainty based on multiple draws from the posterior parameterizations. The Bonnet record spans the deglacial interval, beginning 18.0 thousand years before present (ka) and continuing until 8.5 ka (sediments younger than 8.5ka are present, but were not analyzed here). Temperature reconstructions generated from brGDGTs extracted following the newer methods first described in De Jonge et al. (2013) and later refined in Hopmans et al. (2016) are compared to 1) an existing brGDGT

record from Silver Lake, Ohio (Watson et al. 2018) and 2) a new lower-resolution brGDGT record from Silver Lake that uses the Hopmans et al. (2016) extraction method. All resulting temperature reconstructions are used to infer relationships between temperature change and vegetation turnover, particularly the existence of any lead-lag relationships with the establishment of no-analog communities, both locally and regionally.

Research Questions and Hypotheses

(1) How congruent are brGDGT temperature reconstructions a) among sites in the Great Lakes Region, b) with pollen-based paleoclimatic reconstructions, and c) with Northern Hemispheric temperature records?

H₁₀: The brGDGT temperature reconstruction from Bonnet Lake and Silver Lake have no congruence among sites, regional temperature estimates, or with other Northern Hemispheric records. No synchrony or commonality in temperature patterns in any calibration with any other independent temperature records would suggest that the efficacy of brGDGTs as a temperature proxy is limited in the Great Lakes Region. It would also indicate that brGDGT temperature records are not reproducible – they may be reflecting changes in highly local environmental factors.

H₁₁: brGDGT temperature reconstructions are congruent across sites, but do not agree with regional pollen-based temperature reconstructions or Northern Hemispheric temperature records. Congruence of brGDGT temperature reconstructions across sites would suggest that temperature patterns during the deglaciation were regional in extent and that the regional pollen-based temperature reconstruction may be inaccurate. Furthermore, disagreement with Northern

Hemispheric temperature records would suggest that the climate of the Great Lakes Region was strongly influenced by regional controls, such as dynamics of the nearby Laurentide Ice Sheet.

H₁₂: brGDGT temperature reconstructions are congruent among alternate calibration, detection methodologies, sites, and agree with regional pollen-based temperature reconstructions but do not agree with Northern Hemispheric temperature records. Agreement among all brGDGT temperature estimates and independent pollen-based temperature reconstructions would indicate that brGDGTs are an effective temperature proxy and that pollen-based temperature reconstructions are accurate. Disagreement with Northern Hemisphere records would again indicate the importance of regional controls.

H₁₃: The brGDGT reconstructions are congruent across sites and agree with Northern Hemispheric temperature records, but not with pollen-based temperature reconstructions. This hypothesis might suggest inaccuracies in the pollen-based temperature reconstructions or differences in sensitivity among paleotemperature proxies.

(2) How uncertain are the brGDGT-based reconstructions and how sensitive are they to choice of extraction method and calibration function?

H₂₀: Uncertainty in brGDGT temperature reconstructions is low at both sites and neither the extraction method or calibration have an effect on the uncertainty brGDGT temperature reconstructions. If uncertainty in brGDGT temperature calibrations is low at both sites and across detection methodologies then the temperature estimates are likely robust. This would also suggest that uncertainty is insensitive to changes in calibration and detection methodologies.

H₂₁: The brGDGT temperature estimates have high uncertainty that sources primarily from calibration. High uncertainty resulting primarily from the calibration functions would be

reflected in a large range of temperature estimates in temperature ensemble members. This would indicate that linear calibration functions poorly characterize the brGDGT-temperature relationship. Potential sources of calibration uncertainty could be from poor calibration datasets or the role of other environmental variables affecting the abundance and distribution of brGDGTs.

H₂₂: The choice of brGDGT detection methodology is the primary source of uncertainty in temperature estimates. If brGDGT temperature estimate uncertainty is primarily from the detection methodology, then focus should be placed on improving brGDGT detection in lake sediments to improve temperature estimate precision.

(3) Did no-analog plant communities establish synchronously in the Great Lakes Region?

Was their establishment driven by regional temperature change?

H₃₀: Periods of abrupt temperature had no effect on the establishment of no-analog vegetation.

No-analog communities establishing without a preceding temperature change would indicate that regional and local temperature was not a primary driver of the development of no-analog communities.

H₃₁: Site-specific establishment of no-analog vegetation is preceded by site-specific temperature change. Temperature changes at Bonnet or Silver Lakes occurring prior to the establishment of no-analog communities would be consistent with the hypothesis that local temperature and site-specific factors were important controlling no-analog community establishment.

H₃₂: No-analog community establishment is regionally synchronous and preceded by regional temperature change. If no-analog community establishment is synchronous across the two study sites and regional temperature change precedes establishment, then site-specific factors are likely

less important than regional climate in determining the composition of vegetation assemblages and the establishment of no-analog communities.

Background and Literature Review

Deglacial Climate History: Last Glacial Maximum to Early Holocene

The last glacial maximum (LGM) is defined as the period in time where ice sheets were at their maximum extent during the previous glaciation (Clark et al. 2009, Denton et al. 2010). The period following the end of the LGM is punctuated by several episodic and abrupt climatic changes of varying magnitudes (Bond et al. 1992, Bond and Lotti 1995, Dansgaard et al. 1993). The Heinrich 1 ice discharge event (H1) (Heinrich 1988) was the first of these abrupt transitions, which shut off deep water formation in the North Atlantic and led to moderate cooling in high northern latitudes (Liu et al. 2009). This was followed by the Bølling-Allerød, a warming of the North Atlantic and Northern Hemisphere at 14.7 ka (Broecker 1998, Lemieux-Dudon et al. 2010). The Younger Dryas followed and brought a return to cold stadial conditions (Alley 2000, Steffensen et al. 2008) in the Northern Hemisphere. Deglaciation was completed by 11.7 ka, marking the transition into the Holocene, the current interglacial (Becker et al. 1991, Birks and Ammann 2000). Each of these abrupt changes had differing impacts across the entire climate system, often with opposite impacts in different hemispheres (Broecker 1998). Less is known about the climatic effects in interior North America, but vegetation records reconstructed from fossil pollen throughout eastern North America show general agreement with ice core data from Greenland and Antarctica (Dahl-Jensen et al. 1998, Viau et al. 2006). Site-level reconstructions in the Great Lakes Region also indicate that local controls on vegetation may differ from

hemispheric climate change, often attributed to local climatic effects of the receding Laurentide Ice Sheet (LIS) (Gonzales and Grimm 2009, Watson et al. 2018, Williams et al. 2004).

The trigger for deglaciation is still uncertain, but apparently deglaciation began in the North Hemisphere with rising summer insolation and initial melting of Northern Hemisphere ice sheets, followed by global warming through an addition of atmospheric CO₂, likely released from the southern Atlantic and Southern Ocean as ocean stratification decreased (Shakun et al. 2012, WAIS Divide Project Members 2015). Greenhouse gas (GHG) forcing is the most important climatic control on global warming since the end of the LGM (Clark et al. 2012). Outgassing of CO₂ from the Southern Ocean and southern Atlantic Ocean first requires ice melt from the Northern Hemisphere ice sheets, which may have been particularly unstable on the principle that ice sheet instability increases with increasing size (Clark 1994, Clark et al. 2012, Denton et al. 2010, MacAyeal 1993). When an ice sheet reaches its largest size, isostatic depression is greatest. This, combined with increasing Northern Hemisphere summer insolation, moves the equilibrium line further north, generating glacial melt and calving events (Denton et al. 2010). The resulting freshwater input into the North Atlantic, near the formation of North Atlantic Deep Water (NADW), could decrease surface water density enough to slow or stop the Atlantic Meridional Overturning Circulation (AMOC). AMOC is responsible for bringing ~30% of the Northern Hemisphere's heat energy to higher latitudes, so any slowdown results in this heat being retained in the south (Wunsch 2005), a phenomenon termed the "bipolar seesaw" (Broecker 1998). Additional oceanic heat in the southern Atlantic contributes to melting sea ice and making previously ice-covered extents of the Southern Ocean and the southern Atlantic available for CO₂ outgassing.

Heinrich events have occurred seven times over the last 60,000 years and are associated with a large break-up of ice sheets, producing armadas of icebergs into the North Atlantic at semi-regular intervals of 5 to 10 thousand years (kyr) (Bond et al. 1992, Heinrich 1988, Hemming 2004). Ice-rafted debris, the marker for Heinrich events, becomes more frequent in many ocean cores at the start of Heinrich stadial 1 (HS1), a cooler period in the North Atlantic during deglaciation (Stager et al. 2011, Stanford et al. 2011). HS1 culminates with Heinrich event 1 (H1), an iceberg discharge and melting event between 16.5 and 15 ka (Stanford et al. 2011) that may have shut off AMOC entirely (Barker et al. 2009). Heinrich events tend to occur during the coldest part of stadials (Hemming 2004), so rising temperature is an unlikely cause of catastrophic iceberg discharge. Ice sheet binge-purge oscillations have been modelled to generate Heinrich events only through geothermal warming leading to meltwater formation at the bottom of ice sheets, creating a low-friction basal surface and rapid iceflow and discharge into the North Atlantic (MacAyeal 1993).

The imprint of H1 differs across North America. Lake Tulane, Florida tracks Heinrich events closely and each event (H0-H6) is expressed as a rapid increase in *Pinus*, indicating warm and wet intervals, climate conditions that are opposite the cold conditions of the North Atlantic (Grimm et al. 2006). Sediment and artifacts in the Pacific Northwest also indicate warmer and wetter conditions (Sarnthein et al. 2006). This contrasts with pollen records in the lower Great Lakes, New England and Maritime Canada, which show signals of cooling during the Younger Dryas (Levesque et al. 1997, Peteet 2000, Shane and Anderson 1993, Watson et al. 2018).

A prominent feature of the Bølling-Allerød is its rate and magnitude of warming in the Northern Hemisphere, with a 9 to 14°C change occurring in 1 to 3 years in Greenland (Buizert et al. 2014, Liu et al. 2009, Severinghaus and Brook 1999, Steffensen et al. 2008). Most hypotheses

for the causes of the Bølling-Allerød require a resumption of AMOC (Broecker 1998, Liu et al. 2009, Weaver et al. 2003) and increased oceanic heat transport to the Northern Hemisphere. AMOC resuming after a shutoff has been modeled to overshoot glacial-state NADW formation. These hypotheses also predict a new semi-stable interglacial state NADW formation, releasing enough stored heat in the ocean to warm the Northern latitudes by 5°C (Ganopolski and Rahmstorf 2001, Liu et al. 2009). Meltwater Pulse 1A (MWP-1A), which closely followed Bølling-Allerød warming, led to a ~20 m sea level rise in under 500 years, beginning at 14.65 ka (Deschamps et al. 2012, Weaver et al. 2003). Earth system model simulations indicate that a pulse of meltwater this size from the Antarctic Ice Sheet (AIS) could increase the buoyancy of Antarctic Intermediate Water (AAIW), allowing NADW formation to restart and bringing heat to the Northern Hemisphere (Bassett et al. 2005, Deschamps et al. 2012, Weaver et al. 2003). Model simulations also indicate that a steady decline in meltwater forcing from the Northern Hemisphere ice sheets could trigger AMOC resumption (Liu et al. 2009). Irrespective of the driving mechanisms, the Bølling-Allerød warming appears to have affected North American temperature and hydrologic regimes (Gonzales and Grimm 2009, Voelker et al. 2015).

The Younger Dryas stadial followed the Bølling-Allerød warm period, beginning at 12.9 ka and continuing until the start of the Holocene at 11.7 ka (Severinghaus and Brook 1999, Severinghaus et al. 1998). A signal of colder and drier conditions in the Northern Hemisphere is recorded by many proxies and sites (Alley 2000, Shakun et al. 2012, Steffensen et al. 2008). Drier conditions are evident as a large spike in dust deposition in ice cores from the North Greenland Ice Core Project (NGRIP) (Steffensen et al. 2008). Cooling was more gradual than the rate of Bølling-Allerød warming, with the coldest temperature at Greenland recorded as 15°C colder than modern (Alley 2000), but atmospheric patterns were likely altered within 1 to 3 years

(Steffensen et al. 2008). The mechanisms for cooling is contended, but a promising hypothesis invokes a combination of meltwater rerouting and the drainage of glacial Lake Agassiz (Tarasov and Peltier 2005) through the St. Lawrence River (Carlson et al. 2007). These events would have produced enough of a freshwater forcing to slow AMOC and reduce the amount of oceanic heat brought northward.

In New England and the Great Lakes region, the Younger Dryas is manifested as a re-expansion of *Picea* (Petet et al. 1993, Shane and Anderson 1993, Shuman et al. 2002), reinforcing the idea that drying and cooling in Greenland extended as far as the North American midcontinent. Furthermore, lake levels fell at sites in Indiana, New York, and Massachusetts, mirroring the indication of drier conditions produced by pollen-based paleoclimatic reconstructions (Shuman et al. 2001, Shuman et al. 2002). The hydroclimate of midcontinental North America contrasts that of eastern and northeastern North America. Mean annual precipitation, January and July precipitation, and relative humidity apparently increased during the Younger Dryas and then decreased with the onset of the Holocene (Gonzales et al. 2009, Voelker et al. 2015). Warming at the end of the Younger Dryas was very abrupt, representing about 5 to 10°C in a few decades in Greenland (Alley 2000, Severinghaus et al. 1998), marking the beginning of the Holocene and its associated stable temperatures (Voelker et al. 2015).

Vegetation History of the Great Lakes Region

Vegetation patterns in the Great Lakes Region during the deglaciation were individualistic, responding to rising temperatures, increasing seasonality of insolation and likely temperature, changes in other environmental variables, and biotic interactions. Broad-scale patterns during this interval included the northward expansion of *Picea*, *Abies*, and *Pinus* to higher latitudes, the expansion of broadleaf taxa out of southern refugia (Williams 2003), and the

formation of no-analog plant communities (Williams and Jackson 2007, Williams et al. 2001). Site-level patterns followed regional trends closely, but the amplitude of pollen abundance varied as did the rate and timing of change.

The northward expansion of *Picea* is documented across many sites in the Great Lakes region. Shane and Anderson (1993) present pollen records from an array of lakes throughout Ohio and Indiana. At Pyle Site, vegetation assemblages at the earliest portion of are comprised of *Picea*, Poaceae, and Cyperaceae (Shane and Anderson 1993). Low total net arboreal pollen during this interval suggests that vegetation production was likely low in the region until later into the deglaciation. Similar patterns are apparent across eastern North America (Webb et al., 2003) where *Picea* relative pollen abundance averaged 20 to 40% percent at 21.0 ka, with highest concentrations in the North American midcontinent. Increased arboreal pollen production suggests that regional plant productivity increased later into the deglacial and several lakes record high *Picea* relative abundance ranging from 60% to 80% from ~18.0 ka to ~15.0 ka, after which *Picea* relative abundance declined. The duration of the *Picea* decline varies significantly throughout the region, lasting from 0.2 to 2.0 kyr (Gill et al. 2012, Wang et al. 2016, Watson et al. 2018) to decrease to <10%. The timing of the decrease also varies; for instance, at Silver Lake, OH, *Picea* remained abundant until 14.0 ka (Gill et al. 2012), whereas *Picea* declines at other sites such as Stotzel-Leis by ~15.0 ka (Watson et al. 2018). A warming climate may have been the dominant process causing *Picea* to migrate northward, but the rate of decline appears to have been highly dependent on non-linear local-scale processes (Gill et al. 2012, Shane and Anderson 1993).

Prior to the *Picea* decline, vegetation communities composed of coniferous and broadleaf taxa formed throughout the Great Lakes Region (Jackson and Williams 2004, Overpeck et al.

1992). This period began with the expansion of *Fraxinus* from midcontinental North America into the Great Lakes Region at ~16.0 ka and the synchronous establishment of *Ostrya/Carpinus* and *Ulmus* (Webb et al. 2003). These four taxa formed communities with the already present *Picea* and *Abies* to create vegetation assemblages that do not exist at present, called 'no-analog' communities (Williams and Jackson 2007). A peak in common dissimilarity metrics, such as squared-chord distance, define this period, while also quantifying the difference from modern pollen assemblages (Williams and Jackson 2007). Near ~12.0 ka, the species that composed no-analog communities wane in abundance while remaining in the Great Lakes Region (Webb et al. 2003). *Ostrya/Carpinus* pollen is nearly absent after 10.0 ka, yet *Ulmus* remained in the region well into the Holocene (Webb et al. 2003). Charcoal becomes more common in sediments with the establishment of no-analog communities and maintains into the Holocene, suggesting fire-vegetation feedbacks as an important process in these vegetation assemblages (Gill et al. 2009).

At several sites, *Pinus* rapidly increased following the decline of no-analog communities (Gill et al. 2009, Shane and Anderson 1993, Watson et al. 2018). The magnitude of change varied by site, but an increase of 40 to 60% relative pollen abundance is typical (Gill et al. 2012, Gill et al. 2009, Shane and Anderson 1993), with some sites such as Stotzel-Leis recording a smaller increase of 10% (Watson et al. 2018). The increase occurs within a few hundred years and decreases as rapidly to near absence after ~1000 years (Gill et al. 2012, Gill et al. 2009, Watson et al. 2018). The rapid change in *Pinus* abundance is reflected as a peak in vegetation turnover during the deglaciation, only being surpassed by modern anthropogenic change (Jacobson et al. 1987). The actual abundance of *Pinus* on the landscape was likely less than suggested by fossil pollen, as *Pinus* is a prolific pollen producer and frequently dampens signals from any other vegetation (Webb et al. 1981). The decline in *Pinus* is followed by a steady

increase in *Quercus* starting ~12.0 ka with many sites in the region reaching stable abundances of 40 to 60% at 11.0 ka. Vegetation assemblages varied, but from the start of the Holocene to the late Holocene the co-occurring taxa tend to be *Ulmus*, *Acer*, *Carya*, and *Ostrya/Carpinus* (Gill et al. 2012, Shane and Anderson 1993, Wang et al. 2016). All taxa are broadleaf and reflect the warmer, more mesic conditions of the early Holocene. These vegetation assemblages persisted throughout the late Holocene, after which hydrologic variability began to change vegetation composition.

Although many of the above vegetation changes have been linked to rising temperatures and millennial-scale temperature variations during the last deglaciation (Williams et al. 2004), a close linkage has been hampered by a scarcity of independent temperature proxies. Vegetation has been posited to be in dynamic equilibrium with climate at millennial scales (Prentice et al. 1991, Webb 1986), but at decadal to centennial scales, a mixture of fast and disequilibrium processes may interact (Svenning and Sandel 2013, Williams and Burke in press, Williams et al. 2002). The sensitivity of vegetation to numerous environmental variables further hinders the ability to determine the length of lags between climate and vegetation change. Temperature reconstructions from ice cores in Greenland or North Atlantic ocean cores are often used to represent the environmental drivers of late-glacial vegetation change (Gill et al. 2009, Whitlock and Bartlein 1997, Williams et al. 2004, Yu and Eicher 1998), but these comparisons are hampered by the large distance of the source climate data to the site where vegetation is changing. The use of local, independent climate proxies may enable a precise determine of vegetation response times to a changing climate.

brGDGT as a Paleotemperature Proxy

GDGTs are a broad group of both branched (brGDGT) and isoprenoidal (isoGDGT) microbial membrane lipids, found in several phyla of Archaea and Bacteria (Schouten et al. 2013). GDGT synthesis was initially thought to be an evolutionary feature of microorganisms that thrived in extreme environments (Damsté et al. 2007); however, the lipids were more common than expected (Schouten et al. 2013). isoGDGT synthesis is now recognized to be contained largely within the Thaumarchaeota (formerly Crenarchaeota) and Euryarchaeota phyla (Schouten et al. 2013), and are abundant in marine environments (Weijers et al. 2006). Less is known about brGDGT-synthesizing microorganisms, but unlike isoGDGTs, brGDGTs are most abundant in terrestrial environments (Weijers et al. 2006). This distinction in sources is the basis of the Branched and Isoprenoidal tetraether (BIT) index, which quantifies the relative abundance of bacterial and archaeal GDGTs in sediments (Hopmans et al. 2004, Weijers et al. 2006). Unique to brGDGTs, the addition of methyl groups and the number of cyclopentane moieties act to maintain membrane fluidity in response to changing environment conditions (Schouten et al. 2013), which is exploited to reconstruct past environmental conditions (Loomis et al. 2015, Watson et al. 2018, Zink et al. 2010).

Mean annual temperature (MAT) is reconstructed from brGDGTs by determining ratios of differing brGDGT lipids with added methyl groups or cyclopentane moieties to other brGDGT lipids with similar additions (Weijers et al. 2007). Weijers et al. (2007) surveyed 134 soil samples for brGDGT compounds from 90 globally distributed locations and found a correlation of 0.70 between the number of cyclopentane moieties, referred to as the cyclisation ratio of branched tetraethers (CBT) and soil pH. The number of methyl groups, referred to as the methylation index of branched tetraethers (MBT), had a correlation of 0.62 with MAT and soil

pH (Weijers et al. 2007). Blaga et al. (2010) surveyed lake sediments from 82 lakes, three in North America, in which MAT was more poorly correlated to MBT, and noted that further work was needed to better understand the source for lacustrine brGDGTs. Loomis et al. (2014) found that brGDGTs were more highly correlated with seasonal temperatures because brGDGTs are deposited during periods of lake mixing.

Subsequent studies have further tested the brGDGT proxy in different regions and settings. Zink et al. (2010) in New Zealand found similar correlations to Weijers et al. (2007) when reconstructing paleotemperature for one lake. Sun et al. (2011) also confirmed the efficacy of brGDGTs as a temperature proxy in China. More recently, Loomis et al. (2015) presented results of MAT for Lake Tana in northeastern Africa, using a calibration designed for east African lakes. A lake calibration was used because calibrations based on global soil datasets generate a cold bias with a higher root mean squared error of prediction for reconstructed MAT from lake sediments (Loomis et al. 2012). When the BIT index was below 0.5 the reconstructed temperature was more variable, a result of high crenarchaeal abundance relative to brGDGT producing bacteria (Loomis et al. 2015). The application of brGDGTs in such a wide variety of locations support its use as an effective paleothermometer, yet key challenges remain, particularly how to best calibrate fractional abundances of brGDGTs to temperature estimates and how best to quantify calibration uncertainty and measurement error.

Recent methodological advancements in De Jonge et al. (2013) enabled the separation of formerly co-eluting brGDGT isomers by using Alltima Silica columns instead of Cyano columns in high precision liquid chromatography-mass spectrometry (HPLC-MS) analysis. This new methodology separated the 5-methyl and 6-methyl isomers of brGDGT IIa, IIb, IIc, IIIa, IIIb, IIIc (De Jonge et al. 2013, De Jonge et al. 2014). Further methodological refinement in Hopmans

et al. (2016) reduced the need from four Alltima Silica columns to two, reducing cost and time. The separation of a crenarchaeol regioisomer (GDGT-0) was also reported (Hopmans et al. 2016), but the value of this added resolution for temperature reconstruction is limited because GDGT-0 is only used in the BIT index. De Jonge et al. (2014) incorporated 231 soil samples from Weijers et al. (2007) and Peterse et al. (2012) into a global calibration of MAT using the newer methodology and showed that these 5- and 6- methyl isomers were present in most previously assessed calibration soil samples. The added resolution of separating 5- and 6-methyl isomers led to the identification of new relationships of individual brGDGTs to MAT. For instance, the 5-methyl brGDGT IIIc has no relationship with MAT, but the 6-methyl brGDGT IIIc' has a weak, but significant, linear relationship (De Jonge et al. 2014). An inverse pattern is present in brGDGT IIc and IIIa, where the 5-methyl isomer linearly correlates to temperature and the 6-methyl isomer does not (De Jonge et al. 2014). These new relationships were used in updated calibrations to reduce root mean squared error of predicted temperatures (De Jonge et al. 2014) but have yet to be applied to lake sediments to reconstruct past temperature in eastern North America.

In North America, brGDGTs remain a new and mostly untested paleotemperature proxy. Watson et al. (2018) generated and compared a brGDGT temperature record from Silver Lake, Ohio with pollen-based temperature reconstruction from Silver Lake and four other nearby sites. Watson et al. (2018) tested alternative calibration functions and showed that the brGDGT record tracked the pollen-derived temperature well when the Weijers et al. (2007) calibration was used. The onset of the Bølling-Allerød and the Younger Dryas at Silver Lake lagged Northern Hemisphere temperature syntheses (Shakun et al. 2012) by ~300 years in both the pollen based temperature reconstruction and the brGDGT temperature reconstruction (Watson et al. 2018).

However, these analyses used the older methods and did not separate the brGDGT isomers described above.

Study Site

Bonnet Lake (40.66737 N, 82.13957 W) is a 41 ha kettle lake located in the Long Lake Campground in Holmes County, Ohio (Figure 1). Typical bedrock of Holmes County consists of Mississippian and Pennsylvanian sandstones and shales (White and Lamborn 1949). The area was settled by Europeans in the early 1800's, which resulted in the near-complete removal of the original forests (Wilson 1974). By 1887 CE, nearly 80 percent of the land area in Holmes County had been converted to cropland or pasture (Wilson 1974). Vegetation adjacent to the lake is primarily birch (*Betula*), maple (*Acer*), aspen (*Populus*), and spruce (*Picea*) with common lawn grass (*Agrostis*) interspersed on the campground. Land use surrounding the lake is dominantly cropland that produces corn. Patches of water lilies (*Nymphaea*) typically grow nearshore.

The lake was formerly called Long Lake and has been cored twice since 1942 (Potter 1947, Sears 1942). Potter (1947) retrieved 29 feet (8.839 m) of sediment and Sears (1942) retrieved about 30 feet (9.144 m) of sediment. A survey of basal radiocarbon dates from lakes and mires throughout Ohio includes a basal date from Bonnet Lake of 18.2 ka (Glover et al. 2011).

Methods

Core Collection

Three cores were taken on June 2015, by John (Jack) Williams (UW-Madison), Ben Bates (UW-Madison), Kevin Burke (UW-Madison), Yue Wang (UW-Madison), Tom Lowell

(University of Cincinnati), and Jackie Rodriguez (University of Illinois) using a Bolivia and modified Livingston square-rod piston corer. Two locations of the lake were cored. Location 1 was at the deepest basin within the lake and location 2 was situated near the shore. Only sediment from location 1 was analyzed in this thesis. Cores A for location 1 yielded 1488 cm of sediment. Core B included an accidental recore of depths 1008 cm to 1108 cm and was not used in this study. Core C was offset by 50 cm in depth from Core A and yielded 1458 cm of sediment.

All cores were taken to the National Lacustrine Core Facility (LacCore) at the University of Minnesota. The cores were split, imaged, and scanned for magnetic susceptibility and bulk density. The images were then used within the Corelyzer (Ito et al. 2017) program to produce a composite core by visually cross correlating shared stratigraphic horizons in Cores A and C. The composite core produced continuous sediment from 0 cm to 1471 cm with few gaps (Table 2). Gaps are present in the composite core at 108 to 110 cm, 178 to 180 cm, 356 to 360 cm, 454 to 460 cm, 553 to 560 cm, 757 to 760 cm, 1109 to 1124 cm, and 1224 to 1228 cm.

Geochronology

An initial search for macrofossils was performed at LacCore by Jack Williams and Ben Watson and macrofossils were located at 1389 cm, and 1402 cm. A second set of macrofossils was found at depths 846.5 cm, 1125.5 cm, 1306.5 cm, 1364 cm, 1366.5 cm, and 1375.5 cm by Ben Watson and Kate Hayes. Claire Rubbelke and I performed a third search for macrofossils and found several at depths 974.5 cm, 1195.5 cm, 1247.5 cm, and 1255.5 cm. Macrofossils were not used for radiocarbon dating if they were too small or judged to be sourced from aquatic plants, to avoid hardwater effects (Grimm et al. 2009).

A lack of macrofossils between 846.5 cm and 1125.5 cm led to a second round of dating using pollen for radiocarbon dating. Five depths were selected for pollen extraction and radiocarbon dating, at even intervals between bracketing radiocarbon dates. The protocol for chemical processing of raw sediment for pollen concentration followed that of Piotrowska et al. (2004), with slight modification. To minimize contamination by modern carbon, PTFE stir rods were used instead of customary wooden stir sticks. Two cubic centimeters (cc) of sediment were taken at 1cm intervals from 1 to 3 cm above and 1 to 3 cm below the target depth for sampling, totaling 12 cc of sediment for each targeted depth for dating. Samples were first treated with 10% potassium hydroxide (KOH) and placed in a water bath for 5 minutes to remove humics and deflocculate the sediment. The sediment was then strained through a 180 μm sieve, with the fraction $>180 \mu\text{m}$ discarded to remove any large pieces of organic matter. Carbonates were dissolved by adding 10% hydrochloric acid (HCl) to each sample and placing into a hot water bath for 5 minutes. Silicates were digested using 48% hydrofluoric acid (HF) and an hour in a hot water bath. This was followed immediately after with two 10% HCl rinses to remove all siliceous colloidal clumps. Reactive organic material was removed adding 12 mL of a saturation of potassium chlorate (KClO_3) in nitric acid (HNO_3) at a ratio of 1-part KClO_3 by weight to 10-parts HNO_3 by volume (Schulze's solution). Samples were then rinsed with deionized (DI) water until they reached neutral pH. Prior to drying for preservation, a small portion of each sample was analyzed under a microscope to confirm presence of pollen grains.

All material for radiocarbon dating was sent to the Keck Carbon Cycle AMS facility at the University of California, Irvine or the National Ocean Science AMS facility at the Woods Hole Oceanographic Institution. Calibration was performed using the *Bcrhon* R package (Parnell 2014) and the IntCal13 Northern Hemisphere calibration curve (Reimer et al. 2013). An age

model was generated using the R program *bacon* Version 2.3.3 (Blaauw and Christen 2011). *Bacon* utilizes a Bayesian autoregressive model with a gamma process to model sediment deposition in a stratigraphic profile (Blaauw and Christen 2011). *Bacon* operates by first dividing the core into sections and then iteratively estimating the accumulation rate for the entire section (Blaauw and Christen 2011). Section length is defined as a parameter in the model, as well as the calibration curve, minimum, and maximum depth. A section length of 5 cm was selected to maintain model flexibility, as a section length larger than 5 cm would have resulted in a stiffer age-depth model that is unable to process abrupt changes in sedimentation rate (Blaauw and Christen 2011). Minimum and maximum depth were assigned based on the minimum and maximum depth of radiocarbon dates. Model priors are sedimentation rate and memory, where sedimentation rate follows a gamma distribution and memory consists of a beta distribution (Blaauw and Christen 2011). The prior for sedimentation rate is assigned to be 20 yr/cm (Goring et al. 2012). The previously published age-depth models were used for Silver Lake (Gill et al. 2012).

Loss-on-Ignition

Standard loss-on-ignition protocols (Heiri et al. 2001) were followed to determine relative fractions of organic carbon and inorganic carbon in the sediment (Dean 1974). For each 1 cm depth, 1 cc of sediment was subsampled from the composite core. The samples were placed in ceramic crucibles and then left in a muffle furnace at 105°C overnight for drying, followed by 550°C for four hours to remove organic carbon, and 1000°C for two hours to remove inorganic carbon. The remaining sediment was weighed after each treatment, which provided sediment dry weight, weight of organic matter, and weight of inorganic carbon matter, respectively.

Pollen Analysis

Fossil pollen was used to reconstruct vegetation change over time. As a first-pass sampling procedure, pollen subsamples (1 cc) were taken from depths in the composite core every 8 cm between 903.5 cm and 1376.5 cm. After generating a preliminary vegetation reconstruction, further subsamples were taken at 4 cm between 1095.5 cm and 1239.5 cm, to focus on periods of rapid vegetation turnover.

A modification of standard protocols in Faegri et al. (1989) was followed for pollen processing and extraction. Using an autopipetter, 1 mL of pollen spike suspension was added to each sample composed of 25% KCl with a concentration of 5.0×10^4 polystyrene spheres/mL to determine pollen influx (Davis et al. 1973). Unless otherwise noted, all subsequent steps performed included centrifugation at 3000 rpm and, at minimum, two rinses of 15 mL DI water. Pollen spiking was followed by an addition of 10% HCl and a 5-minute hot water bath to remove carbonates. A 10% KOH treatment followed by 20 minutes in a hot water bath removed humic acids and deflocculated sediments. Silicates were digested by treating the samples with 48% HF placed in a hot water bath for 20 minutes. Sediments that were especially silicate rich followed a different digestion protocol. Samples were left in 48% HF overnight, and the day after were placed in a hot water bath for 20 minutes. Following silicate digestion, sediments were treated twice with 10% HCl in a hot water bath for 5 minutes to disaggregate any siliceous colloidal clumps that may have resulted from silicate digestion. This was followed by two rinses of 6 mL glacial acetic acid to prepare the samples for acetolysis. An acetolysis mixture of 9 parts acetic anhydride to 1 part 32 M sulfuric acid (H_2SO_4) was mixed and 6 mL of this mixture was added to each sample. This step removes all non-sporopollenin substances, which aids identification of morphological features on the pollen grains (Hesse and Waha 1989). An additional rinse in

glacial acetic acid followed the completion of acetolysis. The samples were then dehydrated by rinsing twice with ethanol and twice with tert-butyl alcohol (TbA). Lastly, samples were transferred to ½ dram vials and suspended in silicone oil for permanent storage.

Pollen identification was performed by placing processed samples onto a glass slide and placing under a microscope with bright field lighting and 300x magnification. When necessary individual grains were magnified to 1000x to aid in identification. Taxonomic resolution when identifying pollen varies, and commonly, pollen grains can only be identified to the genus level. However, some pollen grains can be identified to a species level (e.g. *Acer saccharum*, *Acer saccharinum*, *Alnus rugosa*), while others may only be identified to a family level (e.g. Poaceae, Asteraceae). I attempted to maximize taxonomic resolution, identifying to a sub-generic level whenever possible and only resorting to identification to a genus and family level when morphologic characteristics were not visible or not discernable. Pollen identification was aided by both online and published resources: Martin et al. (2017), Kapp et al. (2000), and McAndrews et al. (1973). Any unknown or undifferentiable pollen grains were recorded as such. Each sample was counted to 300 pollen grains, except for 7 samples near core-bottom where pollen concentration was low. In those samples only 200 grains of pollen were counted. Pollen abundance was expressed as a percentage of the total upland sum and was calculated using the program *Tilia* (Grimm 1991). Pollen accumulation rate was also calculated using *Tilia* (Grimm 1991). Stratigraphically constrained incremental cluster analysis (CONISS) was performed using the *rioja* R package (Juggins 2015).

Pollen counts for Silver Lake (Gill et al. 2012) were obtained from the Neotoma Paleoecological Database (www.neotomadb.org) (Williams et al. 2018) using Neotoma Explorer.

The appended pollen diagram includes all taxa that reached a maximum relative abundance of at least 2% of the total upland sum. A total of 120 different pollen types were counted. Many herbaceous taxa did not have relative abundances that exceeded the 2% threshold and were thus summed to a higher taxon (e.g. *Ambrosia*, *Iva*, and others were summed into Asteraceae).

Dissimilarity Analysis

Dissimilarity analysis is frequently used in paleoecology to quantify the difference in fossil pollen assemblages relative to a modern pollen assemblage. Several metrics are available to quantify dissimilarity, and squared-chord distance (Equation 1) has proven to be especially effective at discriminating among pollen samples from different vegetation formations (Overpeck et al. 1985). Squared-chord distance is calculated as:

$$D_{ij} = \sum_y (\sqrt{p_{yi}} - \sqrt{p_{yj}})^2 \quad (1)$$

where y is the total number of taxa chosen for analysis, p is the relative abundance of pollen, i are the fossil samples, and j are the modern samples used for comparison. For each fossil sample, its closest modern analogue was identified and the dissimilarity of that pairing (the minimum dissimilarity) was recorded. Minimum dissimilarity is used as an index of ecological novelty (Radeloff et al. 2015). Dissimilarity calculations in this study use the smaller taxa list from Williams et al. (2001). The threshold for defining samples with no modern analog in this study is set to 0.2 (Jones et al. 2017, Liu et al. 2013, Williams and Shuman 2008). In eastern North American, late-glacial communities with dissimilarities above this threshold are often associated with high abundances of conifers (e.g. *Picea*), broadleaf taxa (e.g. *Ostrya/Carpinus*, *Fraxinus*),

and herbaceous elements (Cyperaceae, *Ambrosia*) (Williams and Jackson 2007, Williams et al. 2001). After pollen relative abundances were calculated for all study sites, dissimilarity was calculated using the R package *analogue* (Simpson 2007). Pollen abundances for the two study sites were summed into pollen types listed by Williams et al. (2001) and compared to all sites in the North American Modern Pollen Database (NAMPD) Version 1.8 using the squared-chord distance metric (Whitmore et al. 2005). The minimum dissimilarity (i.e. most similar) values were then retained for each sample at each lake. Hereafter, minimum dissimilarity will be referred to as novelty (Radeloff et al. 2015).

brGDGT Processing and Analysis

The brGDGT processing was performed at Brown University in the Russell lab, following procedures outlined in Loomis et al. (2012). The sampling design yielded nine samples between 1401.5 cm and 1273.5 cm at 16 cm resolution, 66 samples from 1260.5 to 1000.5 at 4 cm resolution, and 6 samples from 985.4 to 905.5 cm at 16 cm resolution. Samples were freeze-lyophilized and then homogenized using an agate mortar and pestle. The mortar and pestle was cleaned using acetone between samples to ensure that all apolar and polar compounds were removed. The dry, homogenized samples were then mixed with Ottawa silica sand to prevent compaction and channeling of the sediment during lipid extraction. All lipids were extracted from the sediment using a Dionex accelerated solvent extractor (ASE) with a 9:1 solution of dichloromethane:methanol (DCM:MeOH). The resulting solution was dried and weighed to determine the lipid yield from each sample. The lipid extract was then separated into its polar and apolar fraction using an alumina column with 9:1 hexane:DCM and 1:1 DCM:MeOH as eluents. The polar fraction was dried under N₂ and then dissolved in a solution of 99:1 hexane:isopropanol and passed through a 0.45 µm filter. brGDGTs of fully processed samples

were then measured on an Agilent/Hewlett Packard 1100 series liquid chromatograph-mass spectrometer (LC-MS) on two Alltima Silica columns following the protocol outlined in Hopmans et al. (2016). Selective ion monitoring analysis was performed to track m/z 1292, 1050, 1048, 1046, 1036, 1034, 1032, 1022, 1020, and 1018.

To enable comparability between temperature reconstructions resulting from brGDGT detection methods at Silver Lake, 37 archived samples from Watson et al. (2018) were analyzed using the newer methods from Hopmans et al. (2016).

brGDGT Temperature Reconstruction

Four linear transfer functions were tested to generate temperature reconstructions at Bonnet Lake and the subset of samples at Silver Lake (Equations 2-5) (De Jonge et al. 2014). Equations 2-5 all result from regressions of MAT onto various indices that quantify the degree of branching in the brGDGTs (MBT'_{5Me} , MBT') or other measures of the relative abundances for various brGDGT compounds, from a global dataset of 231 soil samples (De Jonge et al. 2014).

$$MAT = -8.57 + 31.45 \times MBT'_{5Me} \quad (2)$$

$$MAT = 5.05 + 14.86 \times Index\ 1 \quad (3)$$

$$MAT_{mr} = 7.17 + 17.1 \times [Ia] + 25.9 \times [Ib] + 34.4 \times [Ic] - 28.6 \times [IIa] \quad (4)$$

$$MAT = 0.81 - 5.67 \times CBT + 31.0 \times MBT' \quad (5)$$

MAT refers to mean annual surface air temperature and MAT_{mr} refers to the calibration resulting from a multiple linear regression (De Jonge et al. 2014). Where Ia, Ib, Ic, and IIa etc. refer to the fractional abundances of individual brGDGT compounds, MBT'_{5Me} (Equation 6), MBT' (Equation 7), and Index 1 (Equation 8), and CBT (Equation 9) are ratios of various brGDGT compounds.

$$MBT'_{5Me} = \frac{Ia + Ib + Ic}{Ia + Ib + Ic + IIa + IIb + IIc + IIIa + IIIa} \quad (6)$$

$$MBT' = \frac{Ia + Ib + Ic}{Ia + Ib + Ic + IIa + IIb + IIc + IIIa + IIIa + IIIa' + IIIa'} \quad (7)$$

$$Index\ 1 = {}^{10}\log \left[\frac{Ia + Ib + Ic + IIIa' + IIIa'}{Ic + IIIa + IIIa + IIIa'} \right] \quad (8)$$

$$CBT = {}^{-10}\log \left(\frac{Ib + IIIb + IIIb'}{Ia + IIIa + IIIa'} \right) \quad (9)$$

I performed uncertainty analysis on the temperature reconstruction by using a Bayesian linear model. De Jonge et al. (2014) performed an ordinary linear regression of mean annual temperature onto MBT'_{5Me} (Equation 6), generating Equation 2. This calibration was chosen for uncertainty analysis as it most closely matched the magnitude of temperature change in the regional pollen-based temperature reconstruction from Watson et al. (2018). I obtained the calibration data from Cindy De Jonge and from this I generated a distribution of possible slopes and intercepts for the regression of MAT onto MBT'_{5Me} . I then sampled from this distribution of possible slopes and intercepts to produce an ensemble of temperature reconstructions. The Bayesian linear model was calculated using the R package *MCMCpack* (Martin et al. 2011), utilizing a Gibbs sampler to take 10,000 draws of a Gaussian distribution for the regression β values and an inverse Gamma distribution for conditional error with uniform priors. I followed an identical procedure for estimating uncertainty in the Weijers et al. (2007) calibration for Silver Lake, obtaining the Weijers et al. (2007) calibration data from the Supplemental Material of the publication.

Results

Geochronology

Two basal radiocarbon dates indicate that accumulation of lacustrine sediments began at 18.0 ka, and 16 additional dates constrain the age-depth relationship until 7.6 ka (Table 1). Glover et al. (2011) show a similar basal age for Bonnet Lake with a basal radiocarbon date of 18.2 ka. The radiocarbon dates associated with depths 1247.5 cm and 1255.5 cm carry uncertainties of +/- 340 and +/- 260 radiocarbon years, respectively, because of small macrofossil size. The associated radiocarbon measurements for depths 1255.5, 1247.5, 1125.5, 975.5, and 846.5 did not include a $\delta^{13}\text{C}$ measurement due to the small size of macrofossils used for dating. Pollen radiocarbon dates have a small uncertainty, but with apparent outliers at two depth intervals (940 cm, 1127 cm) (Table 1, Figure 2), indicating that the isolation of pollen for dating was successful in three of the five samples.

The *bacon* model converged successfully, with a stable trace (Figure 2a). The prior and posterior distributions of the *bacon* for sedimentation rate were closely similar, while the posterior distribution for memory was less than the prior (mean 0.4 vs. mean 0.7). Sedimentation rates across the age-depth relationship are linear and averaged 19 yr/cm with an increase after 1250 cm to 35 yr/cm. Sedimentation rate reaches a minimum of 9 yr/cm at a depth of 1033 cm. This minimum is maintained until 940 cm, after which it increases to 20 yr/cm. Four dates were rejected as outliers, the previously mentioned pollen radiocarbon samples at depths 940 cm and 1127 cm, and two wood fragments at depths 975.5 cm and 1125.5.

Loss-on-Ignition

The mineral fraction of the sediment is high in the lowermost portion of the core, averaging 89% of the sediment by weight until a gradual decline begins at 16.0 ka (Figure 3).

Afterwards, the mineral fraction remains at an average of 78% but contains an excursion at 12.7 ka where values increased to 83% and remained high until 12.2 ka. Inversely, organic matter content in the lake sediments was low initially, averaging 4.75% until 16.0 ka, then increased to an average of 15%, which was maintained well into the early Holocene. An initial peak in inorganic carbonate momentarily occurred at 17.9 ka up to 25% and decreased gradually, coincident with a decrease in the mineral fraction. The percent weight of inorganic carbonate remains generally stable with slight variability at an average 3% from 18 ka until 12.0 ka. The inorganic carbon fraction then gradually increases to 10% until 9.6 ka, after which values drop to 2.5% until 7.5 ka. Both the organic matter and inorganic carbonate content occasionally spike to high relative content, at 1152.5 cm (12.8 ka), 1066.5 cm, (11.0 ka), 1060.5 cm (10.8 ka), 1006.5 (10.1 ka), and 998.5 cm (10.1 ka). During the Holocene, organic matter increases to a peak of 61% at 466 cm followed by a decline to 10% which continues as the average value for the rest of the record (Figure S1).

Vegetation History

Based on the CONISS zonation, four pollen zones were identified (Figure 3):

Zone 1: Picea, Pinus, Abies – This zone is interpreted as a coniferous forest or woodland which was present when the lake formed at 18.0 ka and remains until 14.8 ka. *Picea* is the most abundant pollen type throughout this period with relative abundance reaching a maximum of 89% and averaging ~70%. The end of the zone is marked by declining *Picea*. *Pinus* relative abundance begins at ~15% but slowly declines. *Abies* shows a similar pattern, but relative abundance values are smaller, starting at ~10%. Upland herbs are rare throughout Zone I with a peak in *Artemisia*, reaching 6% relative abundance at ~18.6 ka.

Zone 2: Picea, Fraxinus, Ostrya/Carpinus, Quercus – This zone begins at 14.8 ka and continues until 13.3 ka and is indicative of a no-analog mixed forest or woodland, with high dissimilarity relative to present (ecological novelty) peaking at 0.57 SCD. *Fraxinus* relative abundance begins at ~10% and remains, with slight variability, at this value. Relative abundances of *Ostrya/Carpinus* are 10% at the start of this zone and reach ~20% by 14.5 ka. *Quercus* relative abundance starts at 15%, then increases to 20%.

Zone 3: Pinus, Picea, Quercus, Ulmus – This zone begins with a rapid increase in *Pinus* abundance at 13.3 ka and ends with an equally rapid decline in *Pinus* abundance at 12.0 ka. High *Pinus*, initially low *Quercus* (<10%), low *Picea* (<15%) and *Ulmus* (<10%) relative abundance suggests that this is primarily a pine forest with hardwood elements. Low *Fraxinus* and *Ostrya/Carpinus* relative abundance are reflected in a lowered novelty value throughout the zone, which averages ~0.1. At the end of Zone 3, as *Pinus* declines, *Quercus* increases.

Zone 4: Quercus, Ulmus, Carya – This zone begins at 12.0 ka and continues until the end of the counted pollen record at 8.7 ka. *Quercus* begins the zone with a peak relative abundance of ~60% and maintains this value with minimum variability. *Carya* slowly becomes more abundant throughout the zone, averaging a relative abundance of 10%. *Ulmus* remains at a relative abundance of ~10% with little variability.

Minimum dissimilarity scores (ecological novelty relative to modern pollen assemblages) at Bonnet Lake (Figure 3) are initially low, at 0.09 and maintain this value until 15.5 ka, at which a minimum is reached of 0.04. Novelty then increases to near 0.6 as *Ostrya/Carpinus* and *Fraxinus* pollen abundances increase. After *Ostrya/Carpinus* and *Fraxinus* pollen abundances decline at 13.3 ka, novelty does as well. After the decline in novelty associated with the disaggregation of no-analog communities values remain at 0.2.

brGDGT Temperature Reconstruction

BIT values have been used to determine the source of GDGT producing microorganisms and the temperature signal they reflect (Hopmans et al. 2004, Weijers et al. 2006). BIT values for Bonnet Lake average .984, with values after a depth of 1300 cm averaging .991 (Figure S3). Similar values have been reported in other lake environments, with authors proposing a soil GDGT source (Watson et al. 2018). The resulting temperature reconstruction MAT, not the temperature of the lake waters (Watson et al. 2018). The distribution of brGDGTs are also controlled by soil pH which can affect resulting temperature reconstructions (Weijers et al. 2007). Recent work by Russell et al. (2018) showed that temperature was the primary control on brGDGT temperature reconstructions that result from 5- and 6- methyl brGDGT isomer separation, thus pH likely played a minimal role in controlling the distribution of brGDGTs at Bonnet Lake (Figure S2).

The four temperature calibrations from De Jonge et al. (2014) at Bonnet Lake produce temperature reconstructions that are qualitatively similar. All reconstructions begin with lower temperature until 15.7 ka after which temperatures rise and a plateau is reached at 14.8 ka, with exception of MAT MBT' calibration which plateaus at 14.7 ka (Figure 4). This warm interval is likely associated with the Northern Hemispheric Bølling-Allerød warming. During this warm period, a brief cold interval is recorded at 14.0 ka in all calibrations, after which temperature rebounds. A cold reversal at 13.4 ka is present across all calibrations reflecting Younger Dryas cooling. After a minimum in temperature is reached at 12.1 ka, temperatures increase into the Holocene where they are warmer than the Bølling-Allerød but more variable.

Despite the qualitatively similar patterns of temperature change, the magnitude of temperature change at these intervals differs across calibrations. MAT Index 1 had a magnitude

of change of 2.5°C from late-glacial (prior to 15.7 ka) to Holocene (Figure 4; Table 3). It also indicates a 2.5°C Bølling-Allerød warming and a 0.75°C Younger Dryas cooling. The magnitude of temperature change in the MAT MBT' calibration across the entire record is 5°C. The late-glacial has a similar temperature to the Bølling-Allerød and is 0.5°C warmer than the Younger Dryas. The MAT_{mr} calibration has the smallest temperature change across the entire record and is also the warmest of the four reconstructions. There is little to no Bølling-Allerød warming, with a 1°C Younger Dryas cooling. Warming from the Younger Dryas to the Holocene is 2.3°C.

The ensemble of temperature reconstructions derived from the MAT MBT'_{5Me} calibration indicates a mean temperature change of 4°C from the late-glacial to the Bølling-Allerød (Figure 6). Both the 95% credible interval and the 95% prediction interval vary by an average of +/- 9.8°C at any given temperature estimate. We discuss this uncertainty further below.

The comparison of differing brGDGT detection methodologies at Silver Lake shows that the different LC-MS analytical methods, which do or do not separate 5- and 6-methyl brGDGT isomers, produce differing temperature estimates (Figure 5). Temperature estimates from both methods begin with warming temperatures until a peak is reached at ~13.1 ka. The 'new method' records peak warming 200 years earlier than the published 'old method' temperature reconstruction from Watson et al. (2018) (Figure 5). Peak warming is immediately followed by Younger Dryas cooling. A minimum in this cold reversal occurs at 12.1 ka which is followed by warming temperatures into the Holocene.

The new detection method produced consistently warmer temperatures across all but the Index 1 calibration. MAT MBT'_{5Me} is an average of 2°C warmer than the Weijers et al. (2007) calibration, with a total warming of 4.5°C from late glacial to early Holocene. MAT MBT' follows a very similar pattern to MAT MBT'_{5Me} but is warmer still. The record begins at 3.8°C

and with an early Holocene temperature of 11.5°C. MAT_{mr} is the warmest of all calibrations beginning the record at 6.2°C. Temperature for the early Holocene is recorded as 11.4°C.

Temperatures reconstructed from MAT Index 1 are invariant relative to the other calibrations – the calibration warms similarly to all others but temperature then remains constant between 4.5 – 5°C.

Temperature change at Bonnet Lake and Silver Lake across all alternate brGDGT temperature reconstructions precedes the establishment of no-analog communities (Figure 8). The onset of Bølling-Allerød warming is defined as the point at which temperatures begin to increase past the late-glacial average: 15.7 ka at Bonnet Lake and 14.5 ka at Silver Lake (Figure 8). Similarly, the initial point at which novelty begins to increase past the late glacial mean defines the establishment of no-analog communities, which occurs at 15.5 ka and 14.0 ka at Bonnet Lake and Silver Lake, respectively (Figure 8). Comparing the timing of events at both lakes there is an apparent intersite offset of ~1,200 years between the onset of Bølling-Allerød warming and an offset of ~1,500 years for the establishment of no-analog communities. The timing of these site-level temperature changes and corresponding vegetation changes also differs from the hemispheric temperature synthesis produced by Shakun et al. (2012). The midlatitude temperature synthesis indicates that Bølling-Allerød warming begins at ~15.0 ka (Figure 7). This would suggest that the temperature change at Bonnet Lake leads hemispheric temperature change and temperature change at Silver Lake lags hemispheric temperature change. However, uncertainties in age models may complicate this inference.

Discussion

brGDGT Temperature Reconstructions

Trends in MAT derived from the different brGDGT calibrations at Bonnet Lake agree with one another and identify key climatic events recorded elsewhere in the Northern Hemisphere (Clark et al. 2012, Shakun et al. 2012). The four tested calibrations at Bonnet Lake detect patterns consistent with warming associated with the Bølling-Allerød and cooling during the Young Dryas, albeit prior to these events occurring elsewhere in the Northern Hemisphere. The brGDGT reconstructed temperature from Silver Lake exhibits similar, but lagged, patterns suggesting that comparability across sites is possible (Watson et al. 2018). Furthermore, these patterns are largely insensitive to differing brGDGT detection methodologies (Figure 5) and temperature trends remain constant across sites and calibrations.

However, important differences exist between the brGDGT temperature records at these two sites. First, the timing of temperature changes associated with the Bølling-Allerød and Younger Dryas varies (Figure 7). Bølling-Allerød warming at Bonnet Lake precedes that of Silver Lake, by ~1,200 years (Figure 7). Temporal uncertainty is perhaps the most reasonable explanation for this offset. Bonnet Lake and Silver Lake are only 145 km apart (Figure 1) and temperature changes are often regional in extent, hence it is unlikely that these two sites experienced such an offset in temperature change. Furthermore, radiocarbon dates do not closely bound this time interval at either Bonnet Lake (Table 1) or Silver Lake (Gill et al. 2012) which reinforces the likelihood that this timing offset is from temporal uncertainty. Looking to the age-depth model for Bonnet Lake, the 95% credible interval for the onset of the Bølling-Allerød is 15.7 ka +/- 530 years (Figure 2). At Silver Lake, the dating uncertainty for the onset of Bølling-Allerød warming is 14.5 ka +/- 460 years (Gill et al. 2012). There is still an offset in the timing

of the Bølling-Allerød when high temporal uncertainty is assumed, suggesting that there are age uncertainties beyond what is quantified by the age-depth model.

Second, the calibrations at Bonnet Lake differ in their absolute values and in the relative magnitude of total late-glacial to Holocene temperature change. The difference in maximum temperature and minimum temperature varies from 3.4°C (MAT_{mr}) to 7.5°C ($MAT\ MBT'_{5Me}$) (Figure 4; Table 3). Minimum and maximum temperature estimates also vary with alternate calibrations and across sites (Table 3). The disagreement in temperature estimates can be attributed to either uncertainties in calibration datasets or the differential response of different brGDGTs used in each calibration (De Jonge et al. 2014, Peterse et al. 2012). Each of the four reconstructions relies on different brGDGT indices (i.e. MBT' , MBT'_{5Me} , etc.) which combine and ratio the relative proportion of several groups of brGDGTs (De Jonge et al. 2014, Weijers et al. 2011, Weijers et al. 2007). The MBT' and MBT'_{5Me} quantify the degree of branching of the brGDGTs, under the theory that branched is an adaptation to maintain a homeoviscous cell membrane, whereas Index 1 is a ratio of brGDGTs generated by randomly testing the correlation of all possible ratios of the 15 5- and 6-methyl brGDGT isomers to MAT. One of the calibrations, MAT_{mr} , uses the relative abundance of brGDGT in generating a relationship with MAT, not relying on indices as other temperature calibrations (De Jonge et al. 2014). As indicated in De Jonge et al. (2014) and Peterse et al. (2012) different brGDGT molecules show different and sometimes opposite responses to temperature. Furthermore, the relationships of some of these molecules to MAT is weak, but still statistically significant (De Jonge et al. 2014, Naafs et al. 2017, Peterse et al. 2012). In light of the different formulations of these calibrations, it can be expected that using different indices would lead to large differences in temperature estimates and consequently different estimates of temperature change. Typical root mean square

error of prediction of brGDGT calibrations to MAT range from $\sim 1.5^{\circ}\text{C}$ to $\sim 5^{\circ}\text{C}$ depending on how measurement error is quantified (De Jonge et al. 2014, Ding et al. 2015, Loomis et al. 2012, Naafs et al. 2017). Including our Bayesian analyses of uncertainty from the linear calibrations suggest a greater temperature uncertainty, $\pm 9.8^{\circ}\text{C}$ for the MAT MBT'_{5Me} calibration from De Jonge et al. (2014) and $\pm 12.3^{\circ}\text{C}$ for the calibration from Weijers et al. (2007). This uncertainty mainly affects the absolute estimates of temperature, while the relative differences in temperature estimates among brGDGT samples are less sensitive but still variable. Assuming that the degree of branching of brGDGTs is related to MAT, as indicated by many studies (De Jonge et al. 2014, Loomis et al. 2012, Loomis et al. 2015, Peterse et al. 2012, Russell et al. 2018, Weijers et al. 2007), changes in MBT'_{5Me} reflect changes in temperature, and thus variations in MBT'_{5Me} index within each record reflect warming and cooling even if the precise temperature changes associated with these variations are uncertain. In other words, patterns such as the deglacial warming leading into the Bølling-Allerød, the Younger Dryas cooling, and within-site lead/lag relationships between temperature and vegetation changes should be robust results, regardless of calibration function, but the actual magnitudes of temperature change remain highly uncertain. The temperature reconstructions from alternative calibrations from Bonnet Lake show a coherent signal – a cold late-glacial, warm Bølling-Allerød, cold Younger Dryas, and warm Holocene (Figure 4). Silver Lake exhibits a similar pattern (Figure 5) indicating that these temperature changes are present throughout the Great Lakes Region and that the brGDGT temperature reconstructions are reproducible across sites. There is no clear independent basis for determining which calibration is more accurate for the Great Lakes Region, this depends on the baseline for what is considered true temperature change. On the basis of magnitude of temperature change throughout the temperature records, the MAT MBT'_{5Me} calibration is closest

to the regional pollen-based temperature reconstruction (Watson et al. 2018) if that taken as the most accurate temperature record, while the MAT MBT' calibration is closest to the Northern Hemispheric temperature synthesis (Shakun et al. 2012) (Figure 7).

Analysis of uncertainty in temperature reconstructions suggests that temperature estimates are variable, but the calibrations can be improved. Uncertainty was the result of the limited explanatory power of the linear models used to generate the temperature calibrations, rather than analytical uncertainty. This could be because the calibration datasets are derived from soil samples which are calibrated to measured air temperature from distant meteorological stations. The microorganisms producing brGDGTs must respond to locally heterogenous soil temperatures where the soil samples were taken, conditions likely not reflected in the instrumental air temperature observations (Schouten et al. 2013). Sampling in these discrete locations is also unlike the averaging inherent in lake sediments as brGDGTs are sourced from the soil surrounding the lake. In the North American lakes studied here, the distribution of the brGDGTs suggests that they are sourced from the soil surrounding the lake, but the lake sediments should integrate soil brGDGTs from the surrounding catchment (Watson et al. 2018). This spatial averaging should mitigate the effects of soil microenvironments on brGDGT reconstructions but cannot remove the variability present in soil samples used in temperature calibrations. Despite this temperature calibration uncertainty, patterns of temperature change are likely reliable and accurate because ensemble members experienced similar temperature patterns (Figure 6). By producing a calibration dataset with precise measurements of environmental conditions at the sampling location this uncertainty should be reduced, unless there are unknown environmental controls on the production of brGDGT compounds.

The magnitude of change for key climatic events also varies between brGDGT detection methodologies and other proxy-based temperature records. Using the older method, Watson et al. (2018) reported a late-glacial to interglacial temperature rise of 11°C , which is approximately double that of the midlatitude temperature synthesis produced by Shakun et al. (2012). The Bonnet Lake samples indicate a smaller temperature change ranging from 2.5°C to 5.4°C during this same interval between 16 ka to 10 ka (Figure 4). The reanalyzed Silver Lake samples only extend to 14.5 ka, but the magnitude of change from the beginning of the record to 10 ka is similar to Bonnet Lake, ranging from 2.2°C to 6.4°C depending on calibration (Figure 5). This disagreement in the magnitude of temperature change between detection methods can be attributed to a differing response of the 5- and 6- methyl isomer brGDGTs to MAT than their coeluting counterparts (De Jonge et al. 2014, Peterse et al. 2012). The smaller temperature change is in better agreement with the Shakun et al. (2012) temperature synthesis which indicates a midlatitude temperature change of 4.7°C (Figure 7). A more striking feature of the reduced temperature change in the newer brGDGT detection methodology is its disagreement with the regional pollen stack (Figure 7) (Watson et al. 2018). While the old detection methodology agrees well with the regional pollen stack (Watson et al. 2018) there is a 5.6°C difference in temperature change between Bonnet Lake temperature estimates using the MAT $\text{MBT}'_{5\text{Me}}$ calibration and the regional pollen stack from 16 ka to 10 ka (Figure 7). It is possible that uncertainty in both the brGDGT and pollen-based temperature reconstructions may impact the difference in magnitude of temperature change. In order to fully assess and accurately determine which temperature reconstruction method is more reflective of true deglacial temperature change in the Great Lakes Region more brGDGT temperature records are a necessity.

Temperature Controls on Late-Quaternary Vegetation Dynamics

At the site-level, vegetation turnover closely tracks changes in temperature. At both sites, the establishment of no-analog communities appears to be closely linked to the warming climate associated with the Bølling-Allerød. However, temperature alone does not explain why these communities were apparently limited to the Bølling-Allerød and did not reappear during the Holocene. Other environmental factors that may have contributed to the formation of these no-analog communities including higher than present seasonality of insolation and temperature, combined with lower than present CO₂ concentrations (Williams and Jackson 2007). Increased seasonality in insolation is controlled by precession which is modulated by obliquity (Huybers 2006), operating at timescales of 23.0 kyr and 41.0 kyr, respectively, with seasonality in the Northern Hemisphere at a low during the LGM and present and at a maximum 11.5 ka. Hence, insolation can be considered largely invariant at the timescales of change involved in the establishment of no-analog communities (i.e. <500 years), but may explain the greater prevalence of no-analog communities during the late Pleistocene and early Holocene relative to the middle to late Holocene (Williams et al. 2007). Changes in the concentration of CO₂ operate at similar timescales to temperature change (Shakun et al. 2012) and may have influenced no-analog community establishment. The lagged onset of no-analog communities at Silver Lake indicates that CO₂ would have changed ~2,000 yrs prior to the establishment of no-analog communities (Figure 8) (Shakun et al. 2012). In addition, no-analog communities at Bonnet Lake established ~500 years before an increase in CO₂ (Figure 9) (Shakun et al. 2012). These offsets appear significant, but as indicated by the brGDGT temperature data there are likely large uncertainties in the age-depth models for Bonnet Lake and Silver Lake suggesting that no-analog communities may have established at a similar time to CO₂ concentration increase. While it is

not possible to parse the effects of temperature change and CO₂ concentration increase on the establishment of no-analog communities at the two study sites a common pattern is visible: after a requisite change in temperature no-analog communities established rapidly, within ~200 years at Bonnet Lake and ~500 years at Silver Lake (Figure 8). While only a speculative hypothesis, the sequence of climatic changes and vegetation changes is consistent with threshold dynamics – a change in temperature between 1.5-5°C at Bonnet Lake and 2-3°C at Silver Lake occurred prior to a large compositional change in vegetation assemblages (Figure 8). Release from megaherbivory may have also influenced the establishment of no-analog communities (Gill 2014, Gill et al. 2012, Gill et al. 2009), but this hypothesis was not evaluated in this thesis. The similarity in the relative series of events across these two study sites implies that temperature change was an important factor in the establishment of no-analog communities.

Environmental requirements and physiological characteristics of *Fraxinus* and *Ostrya/Carpinus* explain why abundance was highest from 15.5 ka to 13.3 ka at Bonnet Lake and Silver Lake. *Fraxinus nigra* and *Ostrya virginiana* are both similarly sensitive to warming temperatures (Fisichelli et al. 2014). In the present temperate-boreal ecotone of northern Minnesota and Wisconsin warming temperatures lead to a linear increase in understory sapling density of both species (Fisichelli et al. 2014). The transition from the cold late-glacial to warmer Bølling-Allerød would have likely generated a similar response. Warmer conditions would have led to greater sapling success and a subsequent increasing in the populations of both species. In addition, Delcourt and Delcourt (1994) show that the high seasonality during the deglacial from 13.0 to 8.0 radiocarbon years before present and of the early Holocene placed *Ostrya virginiana* and *Carpinus caroliniana* at a physiological advantage because of their diffuse-porous wood structure. While *Fraxinus* has ring porous wood (Delcourt and Delcourt 1994) it is shade tolerant

(Loehle 1988) and likely took advantage of an opening forest canopy which resulted from decreasing *Picea* abundance. The 200-500 year lag between temperature change and no-analog community establishment poses a problem when considering the life histories of the typical eastern North America no-analog taxa. *Ostrya virginiana*, *Carpinus caroliniana*, and *Fraxinus nigra* all begin to reproduce between the ages of 25 to 40 years (Loehle 1988), shorter time than the lags shown here. However, the time needed for migration from source locations (Giesecke et al. 2017, Huntley and Birks 1984, Huntley and Webb 1989) and successful establishment of populations large enough to be recorded in the pollen record likely took hundreds of years.

The rise of novel pollen assemblages soon after changes in temperature and during novel climate conditions reinforces the dynamic equilibrium hypothesis proposed by Webb (1986). The brGDGT temperature records from Silver Lake and Bonnet Lake and other climate records support this hypothesis (Figure 8). At Bonnet Lake, the decline in *Picea* does not occur until Bølling-Allerød warming begins at 15.7 ka, lagging warming by 200 years. Similarly, at Silver Lake the decline in *Picea* precedes Bølling-Allerød warming, but by 500 years. These findings are consistent with those of Williams et al. (2001), that vegetation turnover preceded maximum dissimilarity from present climate conditions in paleoclimate model simulations from Community Climate Model version 1.

Similar to the asynchrony in temperature changes in the brGDGT records, the asynchrony in the timing of vegetation turnover at Bonnet and Silver Lake, on the order of 1,500 years, can likely be explained by temporal uncertainty. The 95% credible interval for the establishment of no-analog communities at Bonnet Lake places the true age at 15.5 ka +/- 540 years. Temporal uncertainty at Silver Lake averages ~200 to 500 years with no-analog communities establishing at 14.0 ka (Gill et al. 2012). In addition, radiocarbon dates do not closely bound this time interval

at either lake. The closest radiocarbon dates at Bonnet Lake are from two small wood macrofossils with large uncertainties of ~1,500 calibrated years and do not closely constrain the timing of *Picea* decline and no-analog community establishment (Table 1). The nearest radiocarbon dates at Silver Lake have a small uncertainty, but the period associated with *Picea* decline and no-analog establishment occurs in a 2,000 year gap between macrofossils in the age-depth model (Gill et al. 2012). Assuming high uncertainty in both age-models, the offset in the decline of *Picea* and establishment of no-analog communities is reduced to ~500 years. The brGDGT temperature records from these lakes exhibit a similar offset with temporal uncertainty included. As mentioned previously, temperature changes are often regional in extent, and since these two sites are close to one another is unlikely that they experienced different temperature patterns. If it is assumed that temperature changed synchronously at both sites it is likely that the decline in *Picea* and the establishment of no-analog communities at Bonnet Lake and Silver Lake also occurred synchronously or quasi-synchronously.

Conclusion

This study suggests that brGDGTs are able to produce replicable reconstructions of temperature variations during the last deglaciation in eastern North America, where a temperature reconstruction from Bonnet Lake matches the patterns also present in existing previous record from Silver Lake (Watson et al. 2018). At Bonnet, among the four tested calibrations, the MAT MBT'_{5Me} calibration from De Jonge et al. (2014) shows greatest similarity to both regional pollen and brGDGT reconstructed temperature from Silver Lake (Watson et al. 2018). However, uncertainties in absolute temperature values remain large, due to both choice of calibration function and uncertainty in the calibration functions. The revised brGDGT

reconstructions that use the De Jonge et al. (2014) discriminants of 5- and 6- methyl brGDGT isomers produced warmer temperature estimates at Silver Lake and reduced magnitude of deglacial temperature rise than prior estimates by methods that did not separate 5- and 6- methyl brGDGT isomers (Watson et al. 2018). If brGDGTs are to become a new standard as an independent temperature proxy in lacustrine sedimentary records in eastern North America, new lacustrine calibration datasets are needed.

Ecological change throughout the Great Lake Region differs in timing, but the establishment of no-analog communities is ubiquitous across sites, as is its close linkage to site-level temperature changes. Peak Bølling-Allerød warming at Silver and Bonnet Lakes predate peak ecological novelty by 200-500 years. Younger Dryas cooling predates the decline of no-analog communities at these sites as well. Although the timing of warming and cooling may not be synchronous across sites (with synchronicity difficult to assess due to radiocarbon uncertainty), the relative sequence of events remains similar at these sites. Therefore, local temperature change was likely an important control on no-analog community establishment, but is unlikely to have been the sole determinant.

References

- Alley RB. 2000. The Younger Dryas cold interval as viewed from central Greenland. *Quaternary Science Reviews* **19** (1): 213-26.
- Barker S, P Diz, MJ Vautravers, J Pike, G Knorr, IR Hall, WS Broecker. 2009. Interhemispheric Atlantic seesaw response during the last deglaciation. *Nature* **457**: 1097.
- Bartlein PJ, SP Harrison, S Brewer, S Connor, BAS Davis, K Gajewski, J Guiot, TI Harrison-Prentice, A Henderson, O Peyron, IC Prentice, M Scholze, H Seppa, B Shuman, S Sugita, RS Thompson, AE Viau, J Williams, H Wu. 2011. Pollen-based continental climate reconstructions at 6 and 21 ka: a global synthesis. *Climate Dynamics* **37** (3-4): 775-802.
- Bassett SE, GA Milne, JX Mitrovica, PU Clark. 2005. Ice sheet and solid Earth Influences on far-field sea-level histories. *Science* **309** (5736): 925-8.
- Becker B, B Kromer, P Trumborn. 1991. A stable-isotope tree-ring timescale of the Late Glacial/Holocene boundary. *Nature* **353**: 647.
- Birks H. 1995. Quantitative palaeoenvironmental reconstructions. *Statistical modelling of Quaternary science data Technical Guide* **5**: 161-254.
- Birks HH, B Ammann. 2000. Two terrestrial records of rapid climatic change during the glacial–Holocene transition (14,000– 9,000 calendar years B.P.) from Europe. *Proceedings of the National Academy of Sciences* **97** (4): 1390-4.
- Blaauw M, JA Christen. 2011. Flexible paleoclimate age-depth models using an autoregressive gamma process. *Bayesian analysis* **6** (3): 457-74.
- Blaga CI, G-J Reichert, S Schouten, AF Lotter, JP Werne, S Kosten, N Mazzeo, G Lacerot, JS Sinninghe Damsté. 2010. Branched glycerol dialkyl glycerol tetraethers in lake sediments: Can they be used as temperature and pH proxies? *Organic Geochemistry* **41** (11): 1225-34.
- Bond G, H Heinrich, W Broecker, L Labeyrie, J McManus, J Andrews, S Huon, R Jantschik, S Clasen, C Simet, K Tedesco, M Klas, G Bonani, S Ivy. 1992. Evidence for massive discharges of icebergs into the North-Atlantic Ocean during the last glacial period. *Nature* **360** (6401): 245-9.
- Bond GC, R Lotti. 1995. Iceberg discharges into the North Atlantic on millennial time scales during the last glaciation. *Science* **267** (5200): 1005.

Broecker WS. 1998. Paleocean circulation during the Last Deglaciation: A bipolar seesaw? *Paleoceanography* **13** (2): 119-21.

Buizert C, V Gkinis, JP Severinghaus, F He, BS Lecavalier, P Kindler, M Leuenberger, AE Carlson, B Vinther, V Masson-Delmotte, JWC White, Z Liu, B Otto-Bliesner, EJ Brook. 2014. Greenland temperature response to climate forcing during the last deglaciation. *Science* **345** (6201): 1177-80.

Carlson AE, PU Clark, BA Haley, GP Klinkhammer, K Simmons, EJ Brook, KJ Meissner. 2007. Geochemical proxies of North American freshwater routing during the Younger Dryas cold event. *Proceedings of the National Academy of Sciences* **104** (16): 6556-61.

Clark PU. 1994. Unstable behavior of the Laurentide Ice Sheet over deforming sediment and its implication for climate change. *Quaternary Research* **41** (1): 19-25.

Clark PU, AS Dyke, JD Shakun, AE Carlson, J Clark, B Wohlfarth, JX Mitrovica, SW Hostetler, AM McCabe. 2009. The Last Glacial Maximum. *Science* **325** (5941): 710-4.

Clark PU, JD Shakun, PA Baker, PJ Bartlein, S Brewer, E Brook, AE Carlson, H Cheng, DS Kaufman, Z Liu, TM Marchitto, AC Mix, C Morrill, BL Otto-Bliesner, K Pahnke, JM Russell, C Whitlock, JF Adkins, JL Blois, J Clark, SM Colman, WB Curry, BP Flower, F He, TC Johnson, J Lynch-Stieglitz, V Markgraf, J McManus, JX Mitrovica, PI Moreno, JW Williams. 2012. Global climate evolution during the last deglaciation. *Proceedings of the National Academy of Sciences* **109** (19): E1134-E42.

Cushing EJ. Problems in the Quaternary phytogeography of the Great Lakes Region. 1965. In: Wright HE, Jr., Frey DG, editors. *The Quaternary of the United States*: Princeton University Press.

Dahl-Jensen D, K Mosegaard, N Gundestrup, GD Clow, SJ Johnsen, AW Hansen, N Balling. 1998. Past temperatures directly from the Greenland ice sheet. *Science* **282** (5387): 268-71.

Damsté JSS, WIC Rijpstra, EC Hopmans, S Schouten, M Balk, AJM Stams. 2007. Structural characterization of diabolic acid-based tetraester, tetraether and mixed ether/ester, membrane-spanning lipids of bacteria from the order Thermotogales. *Archives of Microbiology* **188** (6): 629-41.

Dansgaard W, SJ Johnsen, HB Clausen, D Dahljensen, NS Gundestrup, CU Hammer, CS Hvidberg, JP Steffensen, AE Sveinbjornsdottir, J Jouzel, G Bond. 1993. Evidence for general instability of past climate from a 250-kyr ice-core record. *Nature* **364** (6434): 218-20.

Davis MB, L Brukaker, T Webb, editors. Calibration of absolute pollen influx. Symposium of the British Ecological Society; 1973.

De Jonge C, EC Hopmans, A Stadnitskaia, WIC Rijpstra, R Hofland, E Tegelaar, JS Sinninghe Damsté. 2013. Identification of novel penta- and hexamethylated branched glycerol dialkyl glycerol tetraethers in peat using HPLC–MS2, GC–MS and GC–SMB-MS. *Organic Geochemistry* **54**: 78-82.

De Jonge C, EC Hopmans, CI Zell, J-H Kim, S Schouten, JS Sinninghe Damsté. 2014. Occurrence and abundance of 6-methyl branched glycerol dialkyl glycerol tetraethers in soils: Implications for palaeoclimate reconstruction. *Geochimica et Cosmochimica Acta* **141** (Supplement C): 97-112.

Dean W, Jr. 1974. Determination of carbonate and organic matter in calcareous sediments and sedimentary rocks by loss on ignition: comparison with other methods. *Journal of Sedimentary Research* **44** (1): 242-8.

Delcourt HR, PA Delcourt. 1994. Postglacial rise and decline of *Ostrya virginiana* (Mill.) K. Koch and *Carpinus caroliniana* Walt. in eastern North America: predictable responses of forest species to cyclic changes in seasonality of climates. *Journal of Biogeography*: 137-50.

Denton GH, RF Anderson, JR Toggweiler, RL Edwards, JM Schaefer, AE Putnam. 2010. The last glacial termination. *Science* **328** (5986): 1652-6.

Deschamps P, N Durand, E Bard, B Hamelin, G Camoin, AL Thomas, GM Henderson, Ji Okuno, Y Yokoyama. 2012. Ice-sheet collapse and sea-level rise at the Bølling warming 14,600 years ago. *Nature* **483**: 559.

Ding S, Y Xu, Y Wang, Y He, J Hou, L Chen, JS He. 2015. Distribution of branched glycerol dialkyl glycerol tetraethers in surface soils of the Qinghai–Tibetan Plateau: implications of brGDGTs-based proxies in cold and dry regions. *Biogeosciences* **12** (11): 3141-51.

Fægri K, PE Kaland, K Krzywinski. 1989. *Textbook of Pollen Analysis*. John Wiley & Sons Ltd.

Fisichelli NA, LE Frelich, PB Reich. 2014. Temperate tree expansion into adjacent boreal forest patches facilitated by warmer temperatures. *Ecography* **37** (2): 152-61.

Ganopolski A, S Rahmstorf. 2001. Rapid changes of glacial climate simulated in a coupled climate model. *Nature* **409**: 153.

Giesecke T, S Brewer, W Finsinger, M Leydet, RHW Bradshaw. 2017. Patterns and dynamics of European vegetation change over the last 15,000 years. *Journal of Biogeography* **44** (7): 1441-56.

Gill JL. 2014. Ecological impacts of the late Quaternary megaherbivore extinctions. *New Phytologist* **201** (4): 1163-9.

Gill JL, JW Williams, ST Jackson, JP Donnelly, GC Schellinger. 2012. Climatic and megaherbivory controls on late-glacial vegetation dynamics: a new, high-resolution, multi-proxy record from Silver Lake, Ohio. *Quaternary Science Reviews* **34**: 66-80.

Gill JL, JW Williams, ST Jackson, KB Lininger, GS Robinson. 2009. Pleistocene Megafaunal Collapse, Novel Plant Communities, and Enhanced Fire Regimes in North America. *Science* **326** (5956): 1100-3.

Glover KC, TV Lowell, GC Wiles, D Pair, P Applegate, I Hajdas. 2011. Deglaciation, basin formation and post-glacial climate change from a regional network of sediment core sites in Ohio and eastern Indiana. *Quaternary Research* **76** (3): 401-10.

Gonzales LM, EC Grimm. 2009. Synchronization of late-glacial vegetation changes at Crystal Lake, Illinois, USA with the North Atlantic Event Stratigraphy. *Quaternary Research* **72** (2): 234-45.

Gonzales LM, JW Williams, EC Grimm. 2009. Expanded response-surfaces: a new method to reconstruct paleoclimates from fossil pollen assemblages that lack modern analogues. *Quaternary Science Reviews* **28** (27-28): 3315-32.

Goring S, JW Williams, JL Blois, ST Jackson, CJ Paciorek, RK Booth, JR Marlon, M Blaauw, JA Christen. 2012. Deposition times in the northeastern United States during the Holocene: establishing valid priors for Bayesian age models. *Quaternary Science Reviews* **48**: 54-60.

Grimm E. 1991. *Tilia and Tiliagraph*. Illinois State Museum, Springfield.

Grimm EC, LJ Maher, DM Nelson. 2009. The magnitude of error in conventional bulk-sediment radiocarbon dates from central North America. *Quaternary Research* **72** (2): 301-8.

Grimm EC, WA Watts, GL Jacobson, BCS Hansen, HR Almquist, AC Dieffenbacher-Krall. 2006. Evidence for warm wet Heinrich events in Florida. *Quaternary Science Reviews* **25** (17-18): 2197-211.

Heinrich H. 1988. Origin and consequences of cyclic ice rafting in the Northeast Atlantic Ocean during the past 130,000 years. *Quaternary Research* **29** (2): 142-52.

Heiri O, AF Lotter, G Lemcke. 2001. Loss on ignition as a method for estimating organic and carbonate content in sediments: reproducibility and comparability of results. *Journal of Paleolimnology* **25** (1): 101-10.

Hemming SR. 2004. Heinrich events: Massive late Pleistocene detritus layers of the North Atlantic and their global climate imprint. *Reviews of Geophysics* **42** (1).

Hesse M, M Waha. 1989. A new look at the acetolysis method. *Plant Systematics and Evolution* **163** (3): 147-52.

Hopmans EC, S Schouten, JS Sinninghe Damsté. 2016. The effect of improved chromatography on GDGT-based palaeoproxies. *Organic Geochemistry* **93**: 1-6.

Hopmans EC, JWH Weijers, E Schefuß, L Herfort, JS Sinninghe Damsté, S Schouten. 2004. A novel proxy for terrestrial organic matter in sediments based on branched and isoprenoid tetraether lipids. *Earth and Planetary Science Letters* **224** (1–2): 107-16.

Hu FS, HE Wright Jr, E Ito, K Lease. 1997. Climatic effects of glacial Lake Agassiz in the midwestern United States during the last deglaciation. *Geology* **25** (3): 207-10.

Huntley B, HJB Birks. 1984. An atlas of past and present pollen maps for Europe: 0–13000 years ago. *Proceedings of the Prehistoric Society* **50**: 408-9.

Huntley B, T Webb. 1989. Migration: Species' response to climatic variations caused by changes in Earth's orbit. *Journal of Biogeography* **16** (1): 5-19.

Huybers P. 2006. Early Pleistocene glacial cycles and the integrated summer insolation forcing. *Science* **313** (5786): 508-11.

Imbrie J, T Webb. Transfer functions: Calibrating micropaleontological data in climatic terms. 1981. In: Berger A, editor. *Climatic Variations and Variability: Facts and Theories*: NATO Advanced Study Institute First Course of the International School of Climatology, Ettore Majorana Center for Scientific Culture. Dordrecht: Springer Netherlands; 125-34.

Ito E, S Higgins, C Jenkins, J Leigh, A Johnson. 2017. Corelyzer. **Version 2.0.4 RC5**.

- Jackson ST, JT Overpeck. 2000. Responses of plant populations and communities to environmental changes of the late Quaternary. *Paleobiology* **26** (sp4): 194-220.
- Jackson ST, JW Williams. 2004. Modern analogs in Quaternary paleoecology: here today, gone yesterday, gone tomorrow? *Annual Review of Earth and Planetary Sciences* **32** (1): 495.
- Jacobson GL, T Webb III, E Grimm. 1987. Patterns and rates of vegetation change during the deglaciation of eastern North America.
- Jones RA, JW Williams, ST Jackson. 2017. Vegetation history since the last glacial maximum in the Ozark highlands (USA): A new record from Cupola Pond, Missouri. *Quaternary Science Reviews* **170**: 174-87.
- Juggins S. 2015. rioja: Analysis of Quaternary science data. R package version (09-5), The Comprehensive R Archive Network.
- Kapp RO, OK Davis, JE King. 2000. Pollen and Spores. American Association of Stratigraphic Palynologists Foundation, Texas.
- Kutzbach J, R Gallimore, S Harrison, P Behling, R Selin, F Laarif. 1998. Climate and biome simulations for the past 21,000 years. *Quaternary Science Reviews* **17** (6): 473-506.
- Lemieux-Dudon B, E Blayo, J-R Petit, C Waelbroeck, A Svensson, C Ritz, J-M Barnola, BM Narcisi, F Parrenin. 2010. Consistent dating for Antarctic and Greenland ice cores. *Quaternary Science Reviews* **29** (1): 8-20.
- Leng MJ, JD Marshall. 2004. Palaeoclimate interpretation of stable isotope data from lake sediment archives. *Quaternary Science Reviews* **23** (7): 811-31.
- Levesque AJ, LC Cwynar, IR Walker. 1997. Exceptionally steep north–south gradients in lake temperatures during the last deglaciation. *Nature* **385** (6615): 423.
- Liu Y, JJ Andersen, JW Williams, ST Jackson. 2013. Vegetation history in central Kentucky and Tennessee (USA) during the last glacial and deglacial periods. *Quaternary Research* **79**: 189-98.
- Liu Z, BL Otto-Bliesner, F He, EC Brady, R Tomas, PU Clark, AE Carlson, J Lynch-Stieglitz, W Curry, E Brook, D Erickson, R Jacob, J Kutzbach, J Cheng. 2009. Transient simulations of the last deglaciations with a new mechanism for Bølling-Allerød warming. *Science* **325** (5938): 310-4.

- Loehle C. 1988. Tree life history strategies: the role of defenses. *Canadian Journal of Forest Research* **18** (2): 209-22.
- Loomis SE, JM Russell, AM Heures, WJ D'Andrea, JS Sinninghe Damsté. 2014. Seasonal variability of branched glycerol dialkyl glycerol tetraethers (brGDGTs) in a temperate lake system. *Geochimica et Cosmochimica Acta* **144**: 173-87.
- Loomis SE, JM Russell, B Ladd, FA Street-Perrott, JS Sinninghe Damsté. 2012. Calibration and application of the branched GDGT temperature proxy on East African lake sediments. *Earth and Planetary Science Letters* **357–358**: 277-88.
- Loomis SE, JM Russell, HF Lamb. 2015. Northeast African temperature variability since the Late Pleistocene. *Palaeogeography, Palaeoclimatology, Palaeoecology* **423**: 80-90.
- MacAyeal DR. 1993. Binge/purge oscillations of the Laurentide Ice Sheet as a cause of the North Atlantic's Heinrich events. *Paleoceanography* **8** (6): 775-84.
- Marlon JR, N Pederson, C Nolan, S Goring, B Shuman, A Robertson, R Booth, PJ Bartlein, MA Berke, M Clifford, E Cook, A Dieffenbacher-Krall, MC Dietze, A Hessel, JB Hubeny, ST Jackson, J Marsicek, J McLachlan, CJ Mock, DJP Moore, J Nichols, D Peteet, K Schaefer, V Trouet, C Umbanhowar, JW Williams, Z Yu. 2017. Climatic history of the northeastern United States during the past 3000 years. *Clim Past* **13** (10): 1355-79.
- Marsicek J, BN Shuman, PJ Bartlein, SL Shafer, S Brewer. 2018. Reconciling divergent trends and millennial variations in Holocene temperatures. *Nature* **554**: 92.
- Martin AC, WJ Harvey, S Goslee. 2017. The Global Pollen Project: a new tool for pollen identification and the dissemination of physical reference collections. *Methods in Ecology and Evolution* **8** (7): 892-7.
- Martin AD, KM Quinn, JH Park. 2011. MCMCpack: Markov Chain Monte Carlo in R. 2011 **42** (9): 21.
- McAndrews JH, AA Berti, G Norris. 1973. Key to the Quaternary Pollen and Spores of the Great Lakes region. Toronto : Royal Ontario Museum.
- Naafs BDA, AV Gallego-Sala, GN Inglis, RD Pancost. 2017. Refining the global branched glycerol dialkyl glycerol tetraether (brGDGT) soil temperature calibration. *Organic Geochemistry* **106**: 48-56.

Overpeck JT, RS Webb, T Webb. 1992. Mapping Eastern North American vegetation change of the past 18 ka - no-analogs and the future. *Geology* **20** (12): 1071-4.

Overpeck JT, T Webb, IC Prentice. 1985. Quantitative interpretation of fossil pollen spectra - dissimilarity coefficients and the method of modern analogs. *Quaternary Research* **23** (1): 87-108.

Parnell A. 2014. Bchron: Radiocarbon dating, age-depth modelling, relative sea level rate estimation, and non-parametric phase modelling. R package version **4** (1).

Peteet D. 2000. Sensitivity and rapidity of vegetational response to abrupt climate change. *Proceedings of the National Academy of Sciences* **97** (4): 1359-61.

Peteet DM, RA Daniels, LE Heusser, JS Vogel, JR Southon, DE Nelson. 1993. Late-glacial pollen, macrofossils and fish remains in northeastern U.S.A. — The Younger Dryas oscillation: A contribution to the 'North Atlantic seaboard programme' of IGCP-253, 'Termination of the Pleistocene'. *Quaternary Science Reviews* **12** (8): 597-612.

Peterse F, J van der Meer, S Schouten, JWH Weijers, N Fierer, RB Jackson, J-H Kim, JS Sinninghe Damsté. 2012. Revised calibration of the MBT-CBT paleotemperature proxy based on branched tetraether membrane lipids in surface soils. *Geochimica et Cosmochimica Acta* **96**: 215-29.

Piotrowska N, A Bluszcz, D Demske, W Granoszewski, G Heumann. 2004. Extraction and AMS Radiocarbon Dating of Pollen from Lake Baikal Sediments. *Radiocarbon* **46** (1): 181-7.

Potter LD. 1947. Post-glacial forest sequence of north-central Ohio. *Ecology* **28** (4): 396-417.

Powers LA, JP Werne, TC Johnson, EC Hopmans, JSS Damsté, S Schouten. 2004. Crenarchaeotal membrane lipids in lake sediments: a new paleotemperature proxy for continental paleoclimate reconstruction? *Geology* **32** (7): 613-6.

Prentice IC, PJ Bartlein, T Webb. 1991. Vegetation and climate change in eastern North America since the Last Glacial Maximum. *Ecology* **72** (6): 2038-56.

Radeloff VC, JW Williams, BL Bateman, KD Burke, SK Carter, ES Childress, KJ Cromwell, C Gratton, AO Hasley, BM Kraemer, AW Latzka, E Marin-Spiotta, CD Meine, SE Munoz, TM Neeson, AM Pidgeon, AR Rissman, RJ Rivera, LM Szymanski, J Usinowicz. 2015. The rise of novelty in ecosystems. *Ecological Applications* **25** (8): 2051-68.

- Reimer PJ, Bard E, Bayliss A, Beck JW, Blackwell PG, Bronk Ramsey C, Buck CE, Cheng H, Edwards RL, Friedrich M. 2013. IntCal13 and Marine13 radiocarbon age calibration curves 0-50,000 years cal BP.
- Russell JM, Hopmans EC, Loomis SE, Liang J, Sinninghe Damsté JS. 2018. Distributions of 5- and 6-methyl branched glycerol dialkyl glycerol tetraethers (brGDGTs) in East African lake sediment: Effects of temperature, pH, and new lacustrine paleotemperature calibrations. *Organic Geochemistry* **117**: 56-69.
- Sarnthein M, Kiefer T, Grootes PM, Elderfield H, Erlenkeuser H. 2006. Warmings in the far northwestern Pacific promoted pre-Clovis immigration to America during Heinrich event 1. *Geology* **34** (3): 141-4.
- Schouten S, Hopmans EC, Schefuß E, Sinninghe Damsté JS. 2002. Distributional variations in marine crenarchaeotal membrane lipids: a new tool for reconstructing ancient sea water temperatures? *Earth and Planetary Science Letters* **204** (1): 265-74.
- Schouten S, Hopmans EC, Sinninghe Damsté JS. 2013. The organic geochemistry of glycerol dialkyl glycerol tetraether lipids: A review. *Organic Geochemistry* **54**: 19-61.
- Sears PB. 1942. Forest sequences in north central States. *Botanical Gazette* **103** (4): 751-61.
- Severinghaus JP, Brook EJ. 1999. Abrupt climate change at the end of the last glacial period inferred from trapped air in polar ice. *Science* **286** (5441): 930-4.
- Severinghaus JP, Sowers T, Brook EJ, Alley RB, Bender ML. 1998. Timing of abrupt climate change at the end of the Younger Dryas interval from thermally fractionated gases in polar ice. *Nature* **391**: 141.
- Shakun JD, Clark PU, He F, Marcott SA, Mix AC, Liu Z, Otto-Bliesner B, Schmittner A, Bard E. 2012. Global warming preceded by increasing carbon dioxide concentrations during the last deglaciation. *Nature* **484**: 49.
- Shane LCK, Anderson KH. 1993. Intensity, gradients and reversals in late glacial environmental change in east-central north America. *Quaternary Science Reviews* **12** (5): 307-20.
- Shuman B, Bravo J, Kaye J, Lynch JA, Newby P, Webb T. 2001. Late Quaternary water-level variations and vegetation history at Crooked Pond, southeastern Massachusetts. *Quaternary Research* **56** (3): 401-10.

- Shuman B, T Webb III, P Bartlein, JW Williams. 2002. The anatomy of a climatic oscillation: vegetation change in eastern North America during the Younger Dryas chronozone. *Quaternary Science Reviews* **21** (16): 1777-91.
- Simpson GL. 2007. Analogue methods in palaeoecology: using the analogue package. *Journal of Statistical Software* **22** (2): 1-29.
- Stager JC, DB Ryves, BM Chase, FSR Pausata. 2011. Catastrophic drought in the Afro-Asian monsoon region during Heinrich event 1. *Science* **331** (6022): 1299-302.
- Stanford JD, EJ Rohling, S Bacon, AP Roberts, FE Grousset, M Bolshaw. 2011. A new concept for the paleoceanographic evolution of Heinrich event 1 in the North Atlantic. *Quaternary Science Reviews* **30** (9): 1047-66.
- Steffensen JP, KK Andersen, M Bigler, HB Clausen, D Dahl-Jensen, H Fischer, K Goto-Azuma, M Hansson, SJ Johnsen, J Jouzel, V Masson-Delmotte, T Popp, SO Rasmussen, R Röthlisberger, U Ruth, B Stauffer, M-L Siggaard-Andersen, AE Sveinbjörnsdóttir, A Svensson, JWC White. 2008. High-resolution Greenland ice core data show abrupt climate change happens in few years. *Science* **321** (5889): 680-4.
- Sun Q, G Chu, M Liu, M Xie, S Li, Y Ling, X Wang, L Shi, G Jia, H Lü. 2011. Distributions and temperature dependence of branched glycerol dialkyl glycerol tetraethers in recent lacustrine sediments from China and Nepal. *Journal of Geophysical Research: Biogeosciences* **116** (G1): G01008.
- Svenning JC, B Sandel. 2013. Disequilibrium vegetation dynamics under future climate change. *American Journal of Botany* **100** (7): 1266-86.
- Tarasov L, WR Peltier. 2005. Arctic freshwater forcing of the Younger Dryas cold reversal. *Nature* **435**: 662.
- Viau AE, K Gajewski, MC Sawada, P Fines. 2006. Millennial-scale temperature variations in North America during the Holocene. *Journal of Geophysical Research: Atmospheres* **111** (D9): n/a-n/a.
- Viau AE, M Ladd, K Gajewski. 2012. The climate of North America during the past 2000 years reconstructed from pollen data. *Global and Planetary Change* **84-85**: 75-83.
- Voelker SL, P-E Noiro-Cosson, MC Stambaugh, ER McMurry, FC Meinzer, B Lachenbruch, RP Guyette. 2012. Spring temperature responses of oaks are synchronous with North Atlantic conditions during the last deglaciation. *Ecological Monographs* **82** (2): 169-87.

Voelker SL, MC Stambaugh, RP Guyette, X Feng, DA Grimley, SW Leavitt, I Panyushkina, EC Grimm, JP Marsicek, B Shuman, B Brandon Curry. 2015. Deglacial hydroclimate of midcontinental North America. *Quaternary Research* **83** (2): 336-44.

WAIS Divide Project Members. 2015. Precise inter-polar phasing of abrupt climate change during the last ice age. *Nature* **520**: 661.

Wang Y, JL Gill, J Marsicek, A Dierking, B Shuman, JW Williams. 2016. Pronounced variations in *Fagus grandifolia* abundances in the Great Lakes region during the Holocene. *The Holocene* **26** (4): 578-91.

Watson BI, JW Williams, JM Russell, ST Jackson, L Shane, TV Lowell. 2018. Temperature variations in the southern Great Lakes during the last deglaciation: Comparison between pollen and GDGT proxies. *Quaternary Science Reviews* **182**: 78-92.

Weaver AJ, OA Saenko, PU Clark, JX Mitrovica. 2003. Meltwater Pulse 1A from Antarctica as a trigger of the Bølling-Allerød warm Interval. *Science* **299** (5613): 1709-13.

Webb T. 1986. Is vegetation in equilibrium with climate? How to interpret late-Quaternary pollen data. *Plant Ecology* **67** (2): 75-91.

Webb T, SE Howe, RHW Bradshaw, KM Heide. 1981. Estimating plant abundances from pollen percentages: The use of regression analysis. *Review of Palaeobotany and Palynology* **34** (3): 269-300.

Webb T, B Shuman, JW Williams. Climatically forced vegetation dynamics in eastern North America during the late Quaternary Period. 2003. *Developments in Quaternary Sciences*. 1: Elsevier; 459-78.

Weijers JW, S Schouten, OC Spaargaren, JSS Damsté. 2006. Occurrence and distribution of tetraether membrane lipids in soils: implications for the use of the TEX 86 proxy and the BIT index. *Organic Geochemistry* **37** (12): 1680-93.

Weijers JW, P Steinmann, EC Hopmans, S Schouten, JSS Damsté. 2011. Bacterial tetraether membrane lipids in peat and coal: Testing the MBT-CBT temperature proxy for climate reconstruction. *Organic Geochemistry* **42** (5): 477-86.

Weijers JWH, S Schouten, JC van den Donker, EC Hopmans, JS Sinninghe Damsté. 2007. Environmental controls on bacterial tetraether membrane lipid distribution in soils. *Geochimica et Cosmochimica Acta* **71** (3): 703-13.

White GW, RE Lamborn. 1949. Geology of Holmes County. Ohio. Division of Geological Survey.

Whitlock C, PJ Bartlein. 1997. Vegetation and climate change in northwest America during the past 125 kyr. *Nature* **388** (6637): 57.

Whitmore J, K Gajewski, M Sawada, JW Williams, B Shuman, PJ Bartlein, T Minckley, AE Viau, T Webb, S Shafer, P Anderson, L Brubaker. 2005. Modern pollen data from North America and Greenland for multi-scale paleoenvironmental applications. *Quaternary Science Reviews* **24** (16): 1828-48.

Williams J, B Shuman. 2008. Obtaining accurate and precise environmental reconstructions from the modern analog technique and North American surface pollen dataset. *Quaternary Science Reviews* **27** (7): 669-87.

Williams JW. 2003. Variations in tree cover in North America since the last glacial maximum. *Global and Planetary Change* **35** (1): 1-23.

Williams JW, KD Burke. Past abrupt changes in climate and terrestrial ecosystems. in press. In: Lovejoy T., L. H, editors. *Climate Change and Biodiversity*.

Williams JW, EC Grimm, JL Blois, DF Charles, EB Davis, SJ Goring, RW Graham, AJ Smith, M Anderson, J Arroyo-Cabrales, AC Ashworth, JL Betancourt, BW Bills, RK Booth, PI Buckland, BB Curry, T Giesecke, ST Jackson, C Latorre, J Nichols, T Purdum, RE Roth, M Stryker, H Takahara. 2018. The Neotoma Paleoecology Database, a multiproxy, international, community-curated data resource. *Quaternary Research* **89** (1): 156-77.

Williams JW, ST Jackson. 2007. Novel climates, no-analog communities, and ecological surprises. *Frontiers in Ecology and the Environment* **5**: 475-82.

Williams JW, DM Post, LC Cwynar, AF Lotter, AJ Levesque. 2002. Rapid and widespread vegetation responses to past climate change in the North Atlantic region. *Geology* **30** (11): 971-4.

Williams JW, BN Shuman, T Webb. 2001. Dissimilarity analyses of late-Quaternary vegetation and climate in eastern North America. *Ecology* **82** (12): 3346-62.

Williams JW, BN Shuman, T Webb, PJ Bartlein, PL Leduc. 2004. Late-Quaternary Vegetation Dynamics in North America: Scaling from Taxa to Biomes. *Ecological Monographs* **74**: 309-34.

Wilson HD. 1974. Vascular Plants of Holmes County, Ohio. *The Ohio Journal of Science* **74** (5): 277-81.

Wunsch C. 2005. The total meridional heat flux and its oceanic and atmospheric partition. *Journal of Climate* **18** (21): 4374-80.

Yu Z. 2007. Rapid response of forested vegetation to multiple climatic oscillations during the last deglaciation in the northeastern United States. *Quaternary Research* **67** (2): 297-303.

Yu Z, U Eicher. 1998. Abrupt climate oscillations during the last deglaciation in central North America. *Science* **282** (5397): 2235-8.

Yu ZC. 2000. Ecosystem response to lateglacial and early Holocene climate oscillations in the Great Lakes Region of North America. *Quaternary Science Reviews* **19** (17-18): 1723-47.

Zink K-G, MJ Vandergoes, K Mangelsdorf, AC Dieffenbacher-Krall, L Schwark. 2010. Application of bacterial glycerol dialkyl glycerol tetraethers (GDGTs) to develop modern and past temperature estimates from New Zealand lakes. *Organic Geochemistry* **41** (9): 1060-6.

Tables

Lab ID	Composite Core Depth (cm)	¹⁴ C age and 1- σ error	δ^{13} C (‰)	Calibrated median age	95% Calibrated credible interval age range	Dated Material
KCCAMS-180323	846.5	6,720 \pm 80		7,583	7,455 – 7,710	wood fragment
KCCAMS-202582	940	8,985 \pm 25		10,191	10,152 – 10,222	pollen
KCCAMS-187203	975.5	13,105 \pm 30		15,735	15,647 – 15,810	wood fragment
KCCAMS-202583	988	8,920 \pm 20		10,036	9,939 – 10,173	pollen
KCCAMS-202584	1033	9,150 \pm 20		10,263	10,245 – 10,367	pollen
KCCAMS-180324	1125.5	9,600 \pm 120		10,932	10,598 – 11,202	wood fragment
KCCAMS-202585	1127	7,050 \pm 20		7,891	7,849 – 7,934	pollen
KCCAMS-202586	1187	11,845 \pm 30		13,661	13,686 – 13,737	pollen
KCCAMS-187204	1247.5	13,630 \pm 340		16,461	15,485 – 17,392	wood fragment
KCCAMS-187205	1255.5	13,560 \pm 260		16,362	15,609 – 17,103	wood fragment
KCCAMS-180325	1306.5	14,355 \pm 30	-24.6	17,502	17,435 – 17,566	wood fragment
KCCAMS-180337	1364	14,755 \pm 35	-24.9	17,950	17,891 – 18,013	twig
KCCAMS-180326	1366.5	14,780 \pm 30	-25.0	17,971	17,921 – 18,029	wood fragment
KCCAMS-180327	1375.5	14,780 \pm 30	-28.2	17,971	17,921 – 18,030	wood fragment
NOSAMS-126078	1389	14,800 \pm 45	-24.88	17,992	17,915 – 18,091	wood fragment
NOSAMS-126079	1402	14,850 \pm 45	-25.89	18,043	17,957 – 18,160	wood fragment

Table 1: Organic materials used for radiocarbon dating, their respective ¹⁴C ages, and calibrated ages using the Northern Hemisphere IntCal13 calibration curve (Reimer et al. 2013). Materials were sent to Woods Hole Oceanographic Institute's National Ocean Science Accelerator Mass Spectrometry Laboratory (NOSAMS) and the W. M. Keck Carbon Cycle Accelerator Mass Spectrometry Laboratory (KCCAMS). All ages reported as years before radiocarbon present (1950AD). Depths are reported relative to the top of the composite core.

Composite Depth (cm)	Drive	Drive Depth (cm)
0	1A-1B-1	0
108		108
110	1A-2B-1	2
178		70
180	1C-2L-1	22
250		92
250	1A-3L-1	33
281		63
281	1C-3L-1	16
356		91
360	1C-4L-1	2
454		96
460	1C-5L-1	2
553		95
560	1C-6L-1	2
659		101
660	1C-7L-1	2
757		99
760	1C-8L-1	2
845		87
845	1A-9L-1	32
881		68
881	1C-9L-1	33
934		86
934	1A-10L-1	19
1006		91
1006	1C-10L-1	59
1028		81
1028	1A-11L-1	14
1109		95
1124	1A-12L-1	16
1175		67
1175	1C-12L-1	49
1224		98
1228	1C-13L-1	2
1323		97
1323	1A-14L-1	26
1369		72
1369	1C-14L-1	48
1399		78
1399	1A-15L-1	9
1471		81

Table 2: Building the composite core at location 1 from drives retrieved from cores 1A and 1C at Bonnet Lake. Drive depth refers to the portion of the drive used in the composite core. Drive depths are measured from the top of sediment in each drive.

	Silver Lake			Bonnet Lake		
	Minimum	Maximum	Range	Minimum	Maximum	Range
MAT MBT' _{5Me}	1.7	8.4	6.7	0.8	8.3	7.5
MAT MBT'	3.9	11.6	7.6	4.0	10.2	6.3
MAT Index 1	3.0	5.2	2.2	4.1	8.7	4.6
MATmr	6.2	11.4	5.2	6.8	10.1	3.4
Weijers et al. (2007)	-2.8	10.1	12.9			

Table 3: Summary of alternate brGDGT temperature reconstructions from Bonnet Lake. Maximum and minimum temperatures in Table 3 correspond with maximum and minimum temperatures in Figure 4 for Bonnet Lake and Figure 5 for Silver Lake. All temperatures are in °C.

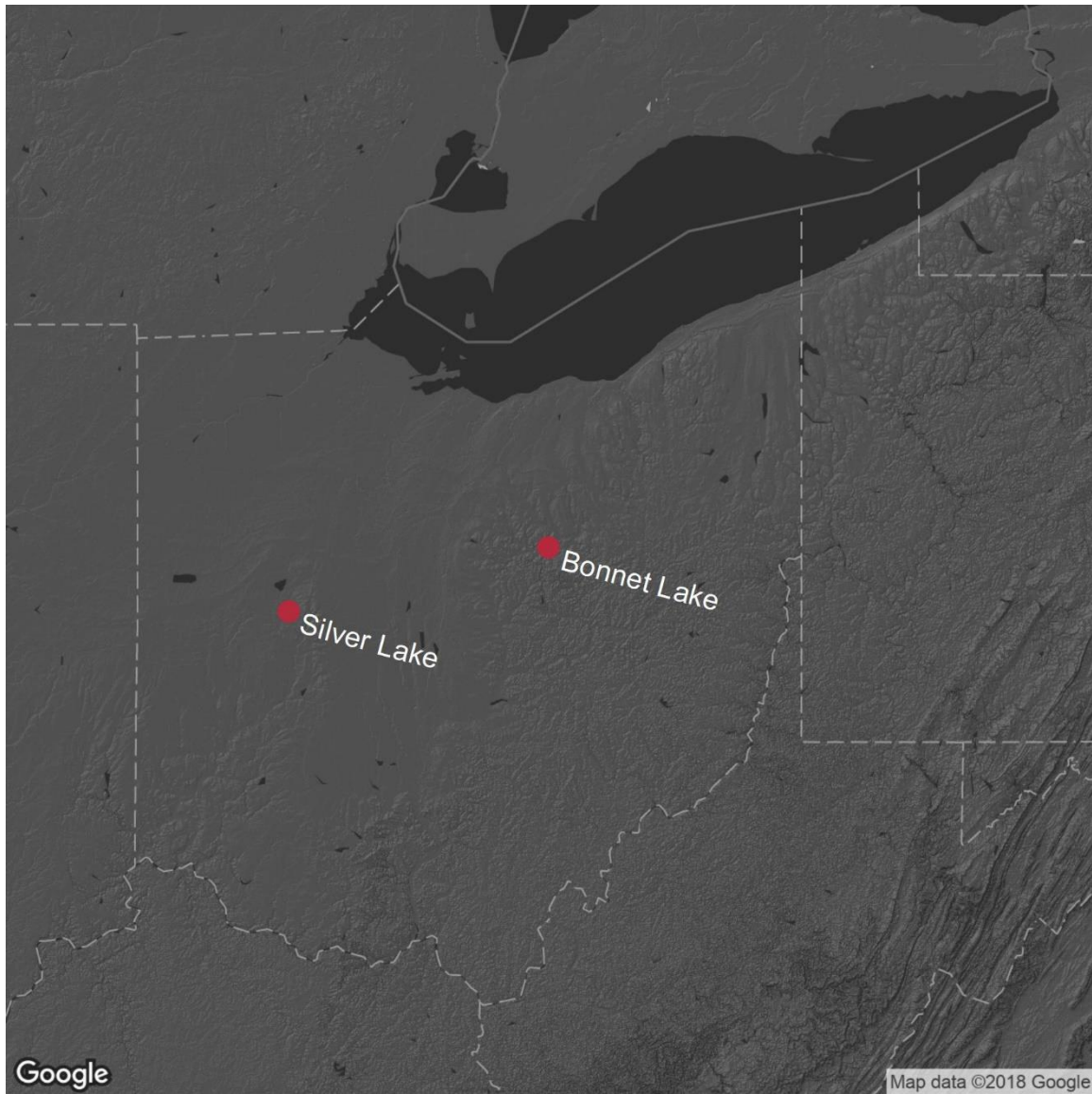
Figures

Figure 1: Map showing locations of Silver Lake and Bonnet Lake. Dashed lines represent state boundaries and solid line represent country boundaries. Topographic relief indicated by shading. Darker shaded areas indicate bodies of water.

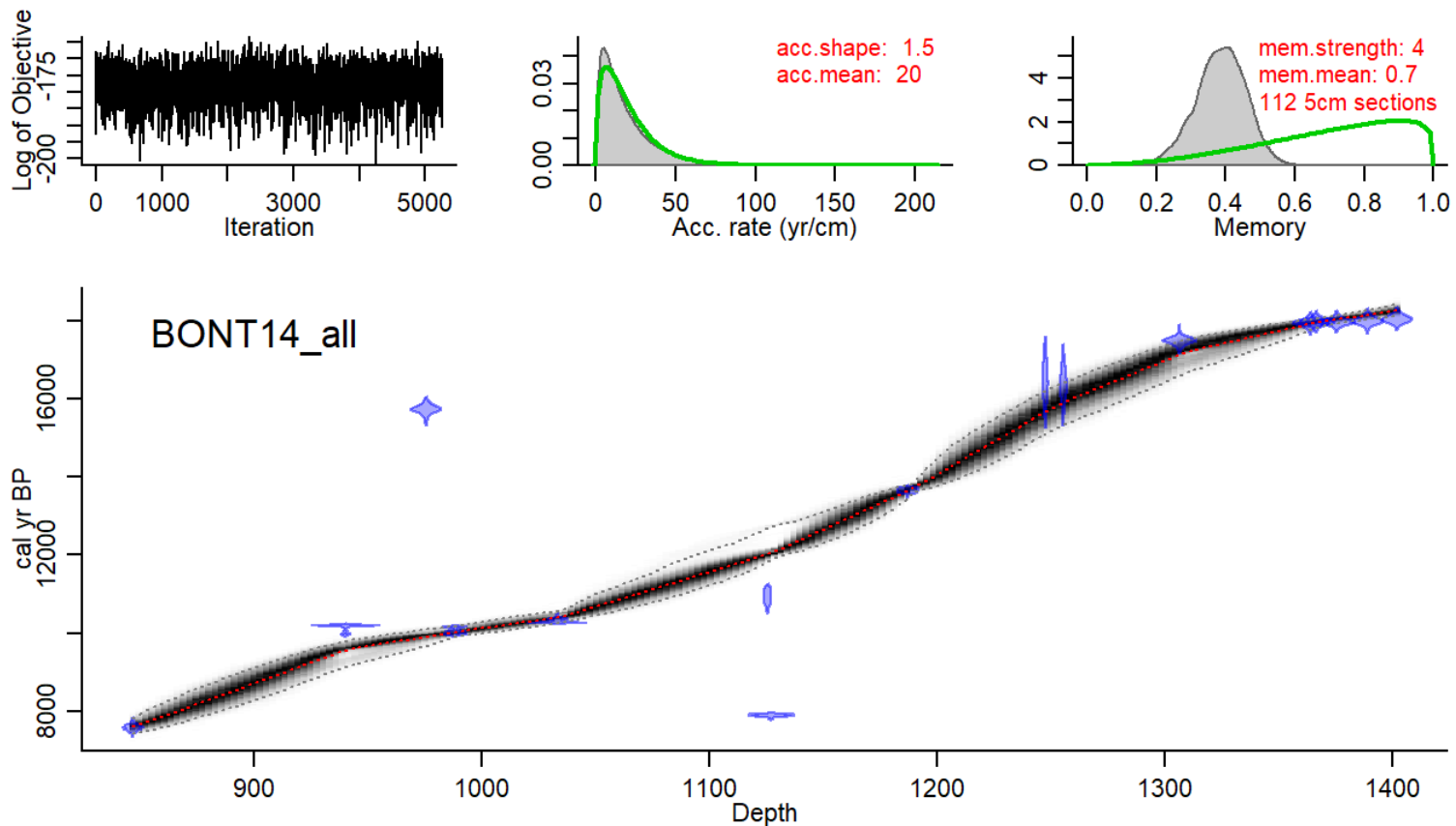


Figure 2: Results from the *bacon* age-depth model for Bonnet Lake, using IntCal13 for the Northern Hemisphere. The upper left plot represents Monte-Carlo Markov chain iterations and indicates model convergence because of stationarity in the distribution of values. The upper-middle plot is the prior (green) and posterior (grey) distribution for the accumulation rate. The upper-right plot is the prior (green) and the posterior (grey) distribution for the memory, i.e. the autocorrelation strength of accumulation rate. The bottom panel shows the age-depth model. The red line is the model ensemble mean estimate, light grey represents the 95% confidence interval, and the darker grey represents likely ages at each depth. Blue violin plots are radiocarbon dates with their calibration distributions. Four dates were rejected by *bacon* as outliers.

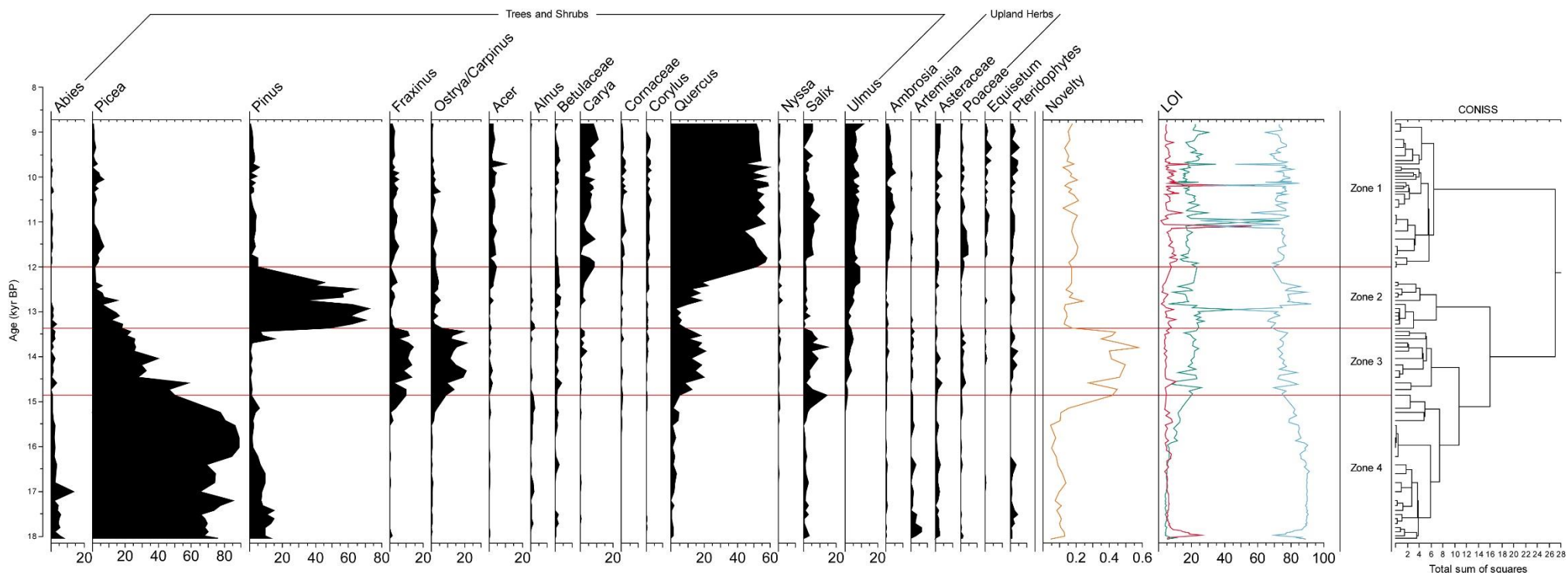


Figure 3: Relative abundance of all pollen types with mean relative abundances at Bonnet greater than 2%. Minimum dissimilarity from present (novelty) was calculated using the minimum squared chord distance of fossil pollen from Bonnet Lake compared to all sites in the North American Modern Pollen Database (Whitmore et al. 2005). Loss-on-ignition plot shows the relative proportion of the mineral fraction (blue), organic fraction (green), and carbonate fraction (red). CONISS was calculated using the *rioja* R package (Juggins 2015).

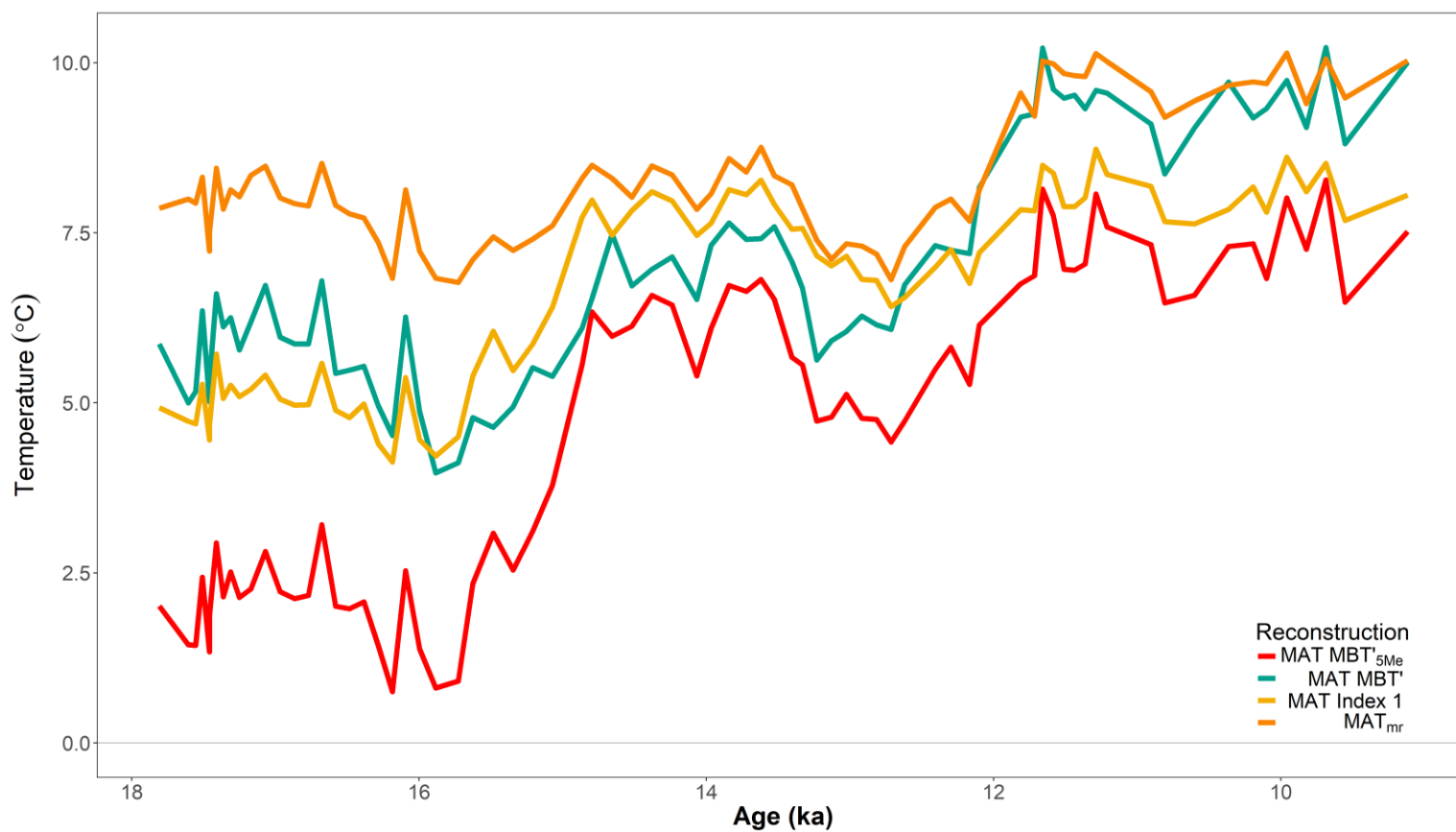


Figure 4: Four possible brGDGT temperature reconstructions for Bonnet Lake, OH using alternative calibrations from De Jonge et al. (2014). The MAT MBT'_{5Me}, MAT MBT', MAT Index 1, and MAT_{mr} reconstructions are based on brGDGT detection methods that are able to separate the 5- and 6-methyl brGDGT isomers (Hopmans et al. 2016).

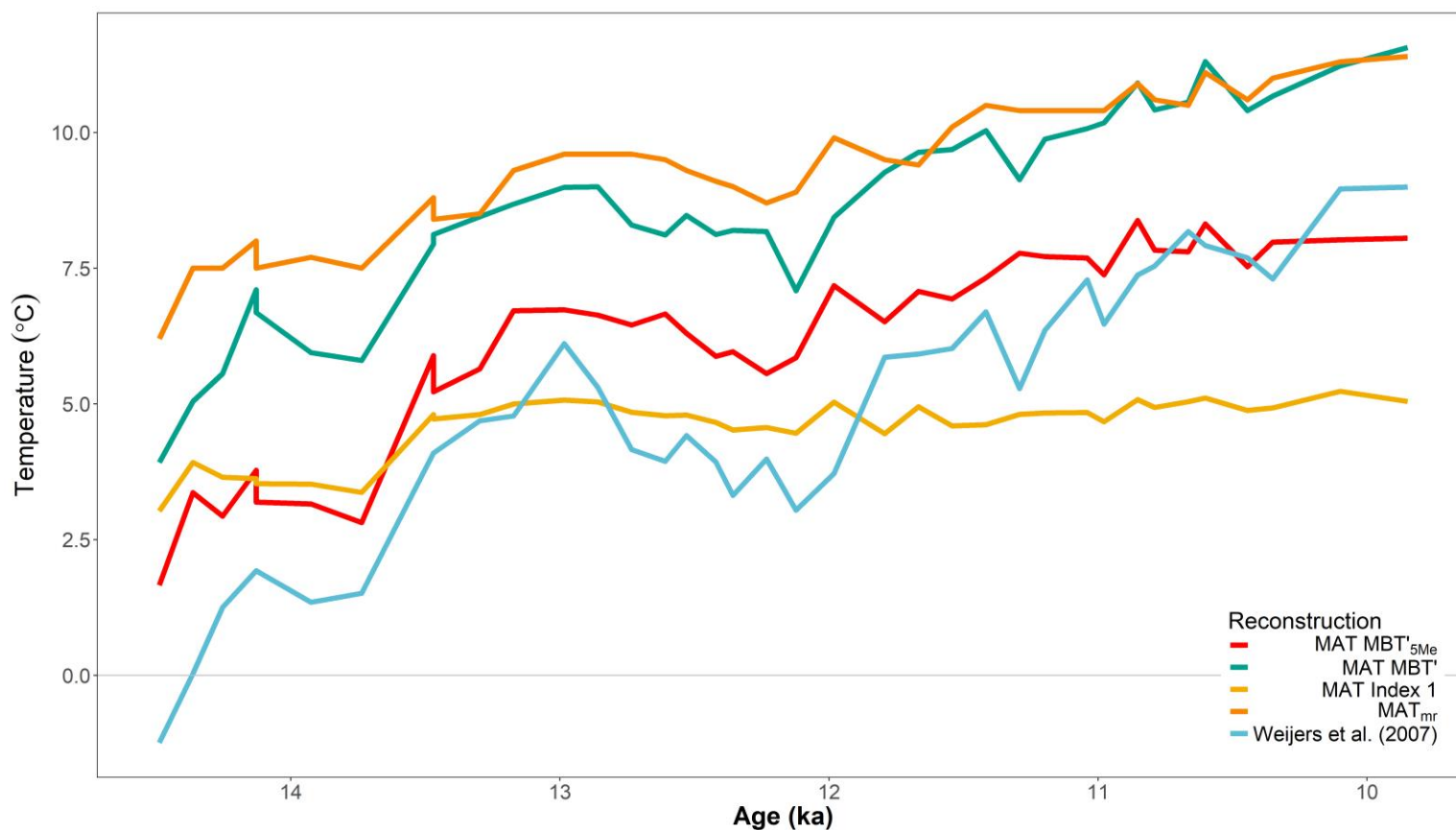


Figure 5: Alternative brGDGT temperature reconstructions for Silver Lake, OH (Watson et al. 2018) using calibrations from De Jonge et al. (2014) and Weijers et al. (2007). The temperature inferences in Watson et al. (2018) are based on the calibration from Weijers et al. (2007); in this thesis we reran a subset of the samples using the brGDGT methods described by Hopmans et al. (2016) and recalculated temperatures using the calibrations from De Jonge et al. (2014). Unlike brGDGT methods used in Hopmans et al. (2016), the calibration from Weijers et al. (2007) results from the use of Cyano columns which are not able to separate 5- and 6-methyl isomers.

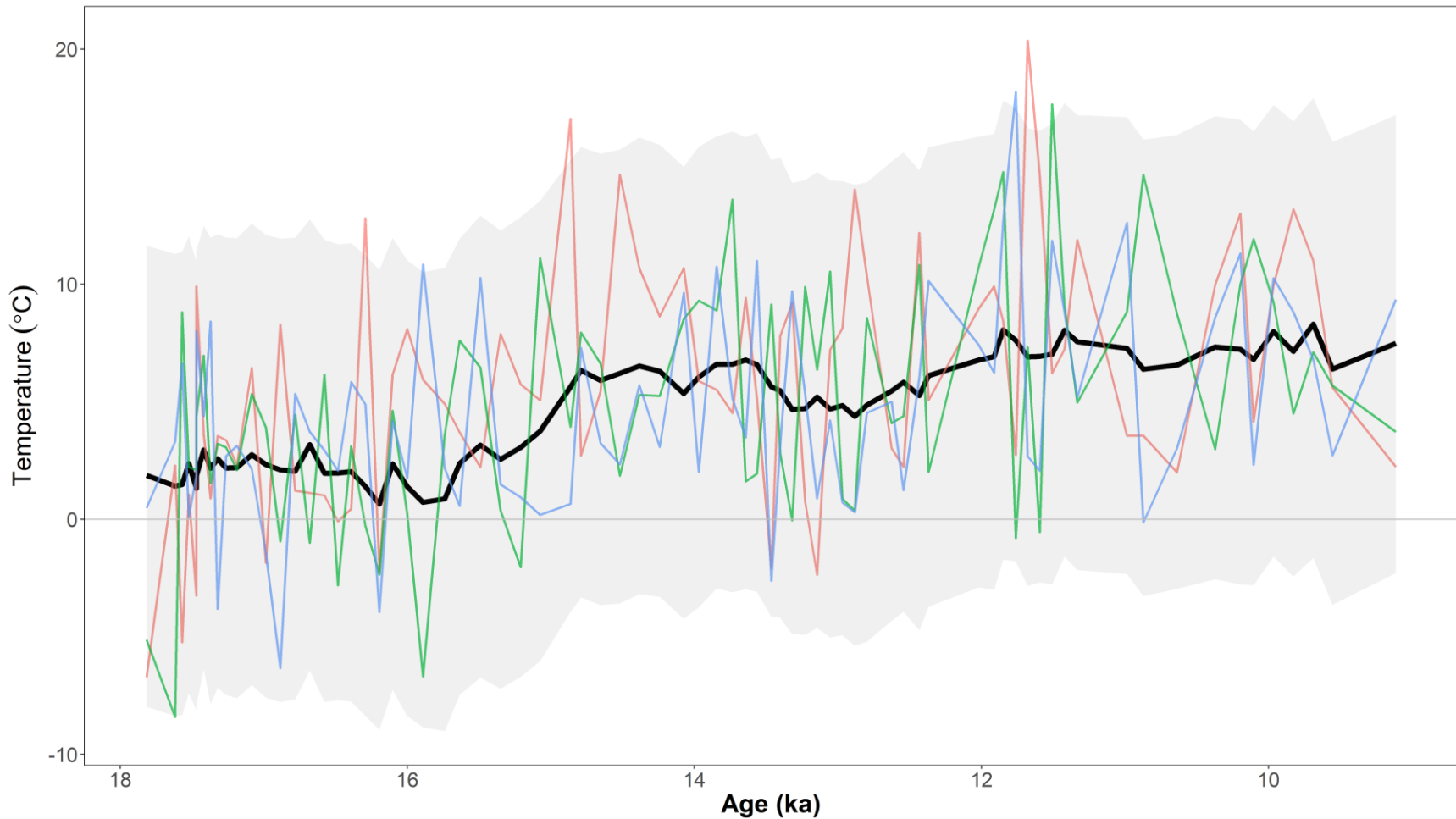


Figure 6: Calibration uncertainty for the MAT MBT'_{5Me} calibration (De Jonge et al. 2014) calculated using a Bayesian linear model instead of an ordinary least squares linear model. The grey area is the 95% credible interval of possible temperatures for all ensemble members. The black line is the median temperature estimate of all ensemble members and the green, red, and blue lines are randomly selected ensemble members.

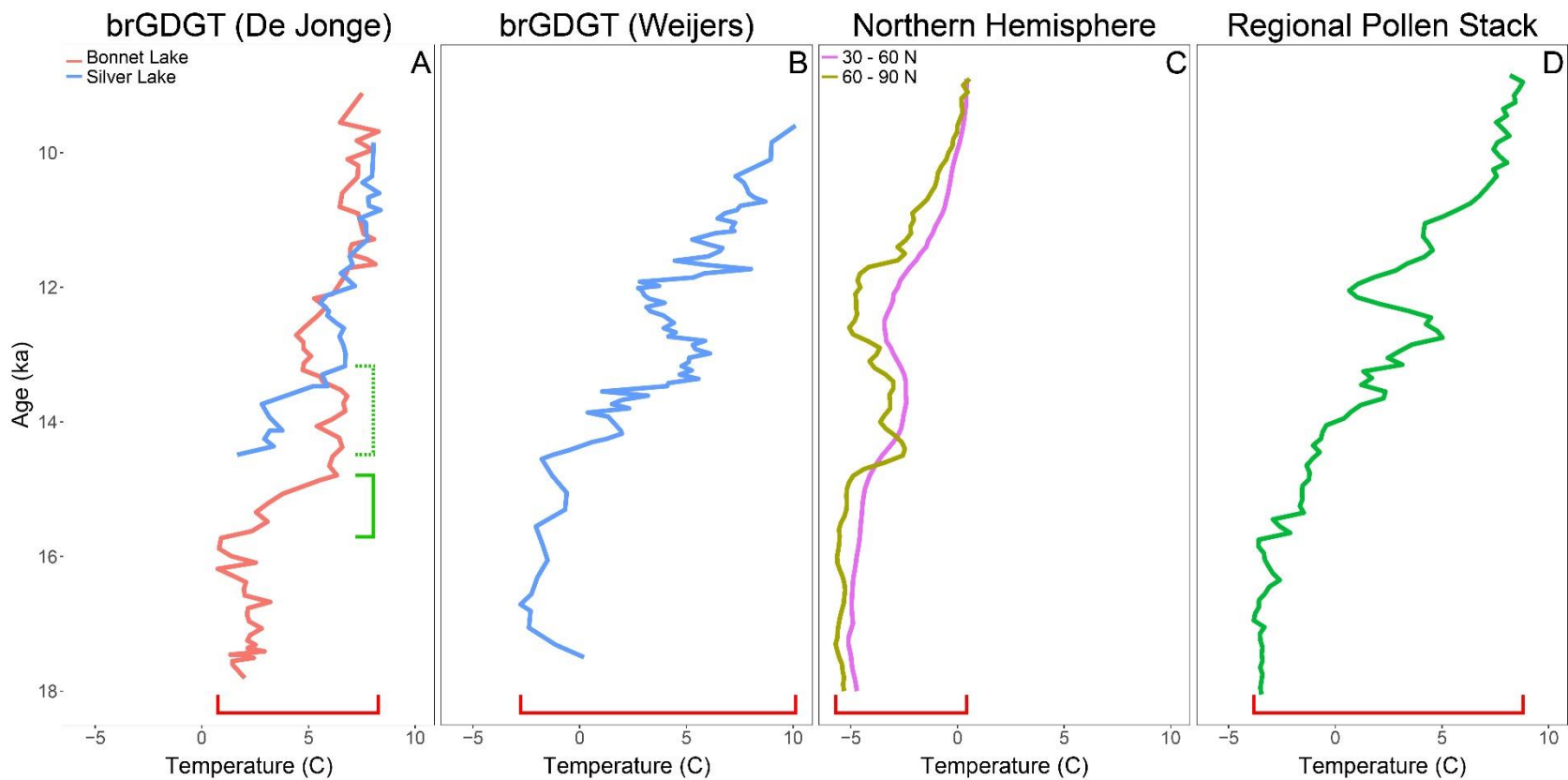


Figure 7: A comparison of temperature trends from different brGDGT detection methods with other proxy records. Red brackets under each plot emphasize the difference in magnitude of total temperature change from the late-glacial to the early Holocene. **(A)** The MAT MBT_{5Me} calibration results from the newer detection method that separate 5- and 6- methyl brGDGT isomers (Hopmans et al. 2016). Only a subset of the original Silver Lake samples were reprocessed using the newer detection method, which is why the MAT MBT_{5Me} temperature reconstruction is shorter than the full temperature record from Watson et al. (2018). The green brackets illustrate the timing offset for the start and end of Bølling-Allerød warming at Bonnet Lake and Silver Lake, with the solid green bracket referring to Bonnet Lake and the dotted green bracket referring to Silver Lake. **(B)** The existing brGDGT temperature reconstructions at Silver Lake (Watson et al. 2018) based on the older detection method and calibrated using functions in Weijers et al. (2007). **(C)** A temperature synthesis for the Northern Hemisphere from Shakun et al. (2012), based primarily on marine temperature proxies. **(D)** A Great Lakes Region temperature estimate produced from a spatially averaged pollen-based temperature reconstruction from five lakes (Watson et al. 2018).

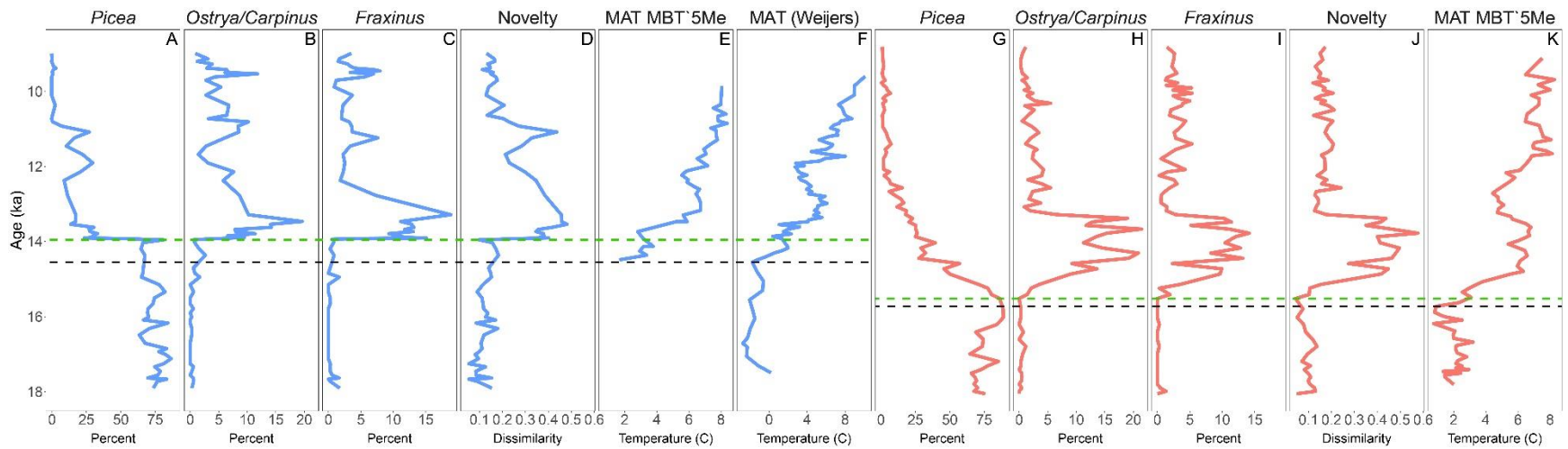
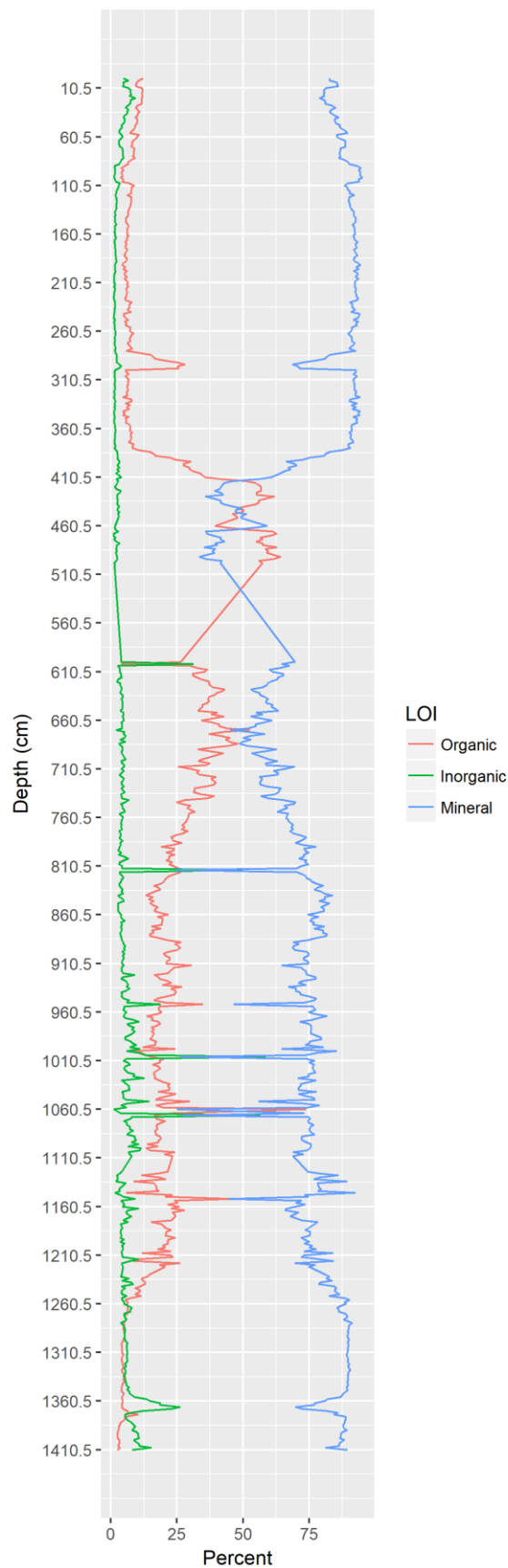


Figure 8: A comparison of temperature trends and the establishment of no-analog communities at Bonnet Lake (red) and Silver Lake (blue). The black horizontal dashed line indicates the start of Bølling-Allerød warming and the green horizontal dashed line indicates the establishment of no-analog communities. **(A-C, G-I)** *Picea*, *Ostrya/Carpinus*, and *Fraxinus* pollen relative abundance are shown because those taxa are major components of the late-glacial no-analog communities of the upper Midwest (Overpeck et al. 1992). **(D, J)** Novelty for Silver Lake calculated using the squared chord distance metric and the entire North America Modern Pollen Database (Whitmore et al. 2005). The novelty curve for Bonnet Lake is reproduced from Figure 3. **(E, K)** brGDGT temperature reconstruction from Bonnet Lake and Silver lake is shown using the MAT MBT'_{5Me} calibration from De Jonge et al. (2014). The Silver Lake MAT MBT'_{5Me} temperature record is truncated because only a portion of the original samples were reanalyzed. **(F)** A brGDGT temperature reconstruction from Watson et al. (2018) calibrated using the Weijers et al. (2007) calibration.

Appendix I. Supplemental Figures

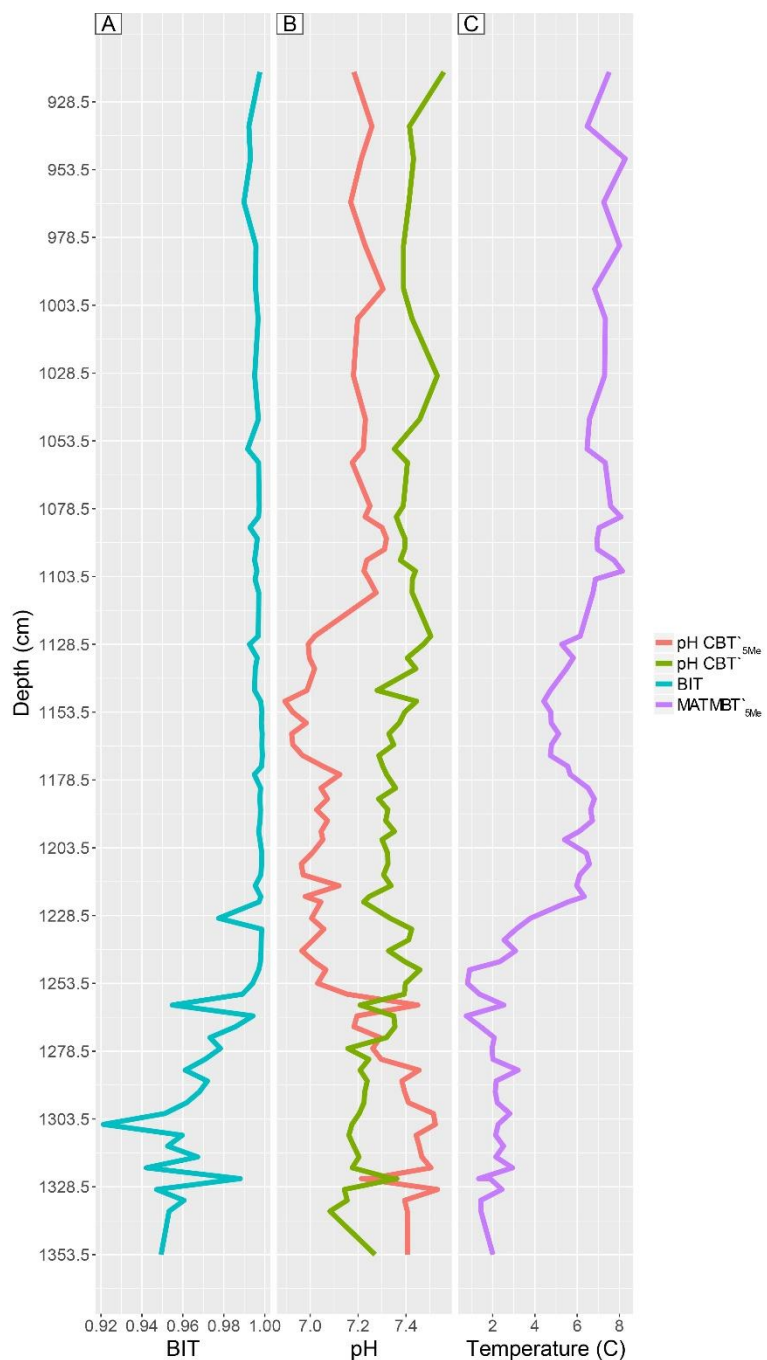
Supplemental Figure 1.

The entire record for loss-on-ignition for Bonnet Lake. A laboratory error is responsible for missing measurements in the inorganic and mineral fraction from 500.5 cm to 598.5 cm. The primary data file was not saved after the mass for the 1000°C burn was entered.



Supplemental Figure 2

(A) Branched and Isoprenoid Tetraether (BIT) index (Hopmans et al. 2004) for Bonnet Lake. BIT remains above 0.90 for the entire record indicating primarily bacterial lipids in the sediments. (B) Reconstructed soil pH for Bonnet Lake using calibrations from De Jonge et al. (2014). (C) Temperature reconstruction from Bonnet Lake using the MAT MBT'_{5Me} calibration from De Jonge et al. (2014). A lack of apparent correlation between pH and temperature suggest that pH was not a large contributor to the reconstructed temperature record.



Appendix II. Bonnet Lake Pollen Counts

Depth (cm)	<i>Abies</i> <i>undiff.</i>	<i>Acer</i> <i>negundo</i>	<i>Acer</i> <i>rubrum</i>	<i>Acer</i> <i>saccharinum</i>	<i>Acer</i> <i>saccharum</i>	<i>Acer</i> <i>undiff.</i>	Agoseris	Alismataceae	<i>Alnus</i>	<i>Alnus</i> <i>crispa</i>	<i>Alnus</i> <i>incana</i>	<i>Ambrosia</i>	<i>Amorpha</i>	<i>Arceuthobium</i>	<i>Arctostaphylo</i> <i>s</i>	<i>Artemisia</i>
903.5	0	4	0	2	0	2	0	0	2	0	0	5	0	0	0	1
911.5	0	1	0	0	1	6	0	0	1	0	0	7	0	0	0	0
919.5	0	3	0	4	0	6	0	0	0	0	0	10	0	0	0	0
927.5	0	1	0	0	0	7	0	0	0	0	0	7	0	0	0	1
935.5	1	0	0	1	0	5	0	1	0	0	0	12	0	0	0	0
943.5	2	0	1	1	0	4	0	0	0	0	0	11	1	0	0	0
951.5	0	33	1	1	0	5	0	0	0	0	0	15	0	1	0	1
959.5	2	2	0	0	1	3	0	0	0	0	0	11	0	0	0	0
967.5	4	1	0	0	0	8	0	0	0	0	0	16	0	1	0	0
975.5	2	2	0	0	0	13	0	0	0	0	0	19	0	1	0	2
982.5	2	0	0	0	2	10	0	0	0	0	0	9	0	0	0	2
991.5	1	2	2	0	0	9	0	0	1	0	0	5	0	0	0	0
999.5	1	3	0	1	0	9	0	0	1	0	0	2	0	1	1	0
1007.5	0	1	0	2	1	6	0	0	1	0	0	3	0	1	0	1
1015.5	3	2	0	2	0	2	0	0	2	0	0	12	0	0	0	2
1023.5	5	2	0	0	1	5	0	0	1	0	0	9	0	0	0	0
1031.5	1	2	0	1	0	7	0	0	3	0	0	15	0	0	0	1
1039.5	0	4	0	1	2	7	0	0	0	0	0	15	0	1	0	0
1047.5	0	2	0	0	5	4	0	0	0	0	0	16	0	0	0	1
1055.5	5	4	0	0	0	3	0	0	2	0	0	8	0	0	0	0
1063.5	3	6	0	0	0	2	0	0	0	0	0	16	0	0	0	0
1071.5	3	5	1	0	0	9	0	0	2	0	0	9	0	0	0	0
1079.5	2	3	0	0	1	4	0	0	0	0	0	9	0	0	0	3
1087.5	3	2	0	0	1	10	0	0	0	0	0	8	0	0	0	0
1095.5	1	5	0	0	0	10	0	0	0	0	0	7	0	0	0	1
1099.5	1	0	0	0	0	1	0	0	0	0	0	5	0	0	0	2
1103.5	2	0	0	1	4	4	0	0	0	0	0	2	0	0	0	0
1108.5	1	2	0	2	6	6	0	0	0	0	0	2	0	0	0	0
1124.5	0	2	1	0	3	3	0	0	0	0	2	1	0	0	0	0
1127.5	1	4	0	0	1	4	0	0	0	0	1	1	0	0	0	0
1131.5	0	0	0	0	0	1	0	0	0	0	2	1	0	0	0	0
1135.5	0	0	0	0	1	0	0	0	0	0	3	0	0	0	0	0
1139.5	0	0	0	0	0	2	0	0	0	1	1	1	0	0	0	0
1143.5	1	2	0	0	3	4	0	0	0	1	4	0	0	0	0	0
1147.5	2	0	0	0	0	1	0	0	0	0	1	4	0	0	0	1
1151.5	5	0	0	0	0	1	0	0	3	0	0	1	0	0	0	1
1155.5	3	0	0	0	0	1	0	0	0	0	0	1	0	0	0	1
1159.5	5	0	0	0	0	0	0	0	1	0	0	1	0	0	0	0
1163.5	2	1	0	0	0	0	0	0	0	0	0	2	0	0	0	3

Depth (cm)	Asteraceae	<i>Betula</i>	Betulaceae	<i>Brassica</i>	Brassicaceae	Cannabaceae	<i>Carex</i>	<i>Carya</i> sp	Caryophyllaceae	<i>Castanea</i>	Celastraceae	<i>Celtis</i>	<i>Cephalanthus</i> sp	Chenopodiaceae	Cornaceae	<i>Cornus</i>	<i>Corylus</i>	Cyperaceae
903.5	6	2	3	0	4	0	0	28	0	0	0	0	0	0	1	0	0	0
911.5	5	0	0	0	6	0	0	33	0	0	0	0	0	0	1	2	0	0
919.5	8	0	2	1	6	0	0	39	0	0	0	0	0	1	1	1	9	0
927.5	9	3	3	0	7	0	1	21	0	0	0	0	0	1	2	3	7	0
935.5	5	1	6	0	2	0	0	32	0	0	0	0	0	1	1	0	1	0
943.5	3	2	8	0	0	0	1	18	0	0	0	0	0	1	6	2	8	0
951.5	7	1	5	0	3	0	0	21	0	0	0	0	0	3	7	2	9	4
959.5	3	1	0	0	0	0	0	22	0	0	0	0	0	0	5	0	3	0
967.5	3	0	1	0	0	0	0	19	0	0	0	0	0	1	6	4	11	0
975.5	8	6	0	0	0	0	0	11	0	0	1	0	0	4	2	4	3	4
982.5	6	2	2	0	0	0	0	8	0	0	0	0	0	0	0	0	1	0
991.5	5	0	7	0	0	0	0	31	0	0	0	0	0	0	4	2	7	0
999.5	2	1	5	0	0	1	1	18	0	0	0	0	0	0	0	1	4	0
1007.5	6	0	0	0	0	0	1	26	0	0	0	0	0	0	4	4	2	3
1015.5	3	1	0	0	0	0	0	29	0	0	0	0	0	0	0	2	8	0
1023.5	0	6	0	0	0	0	0	21	0	0	0	0	0	0	0	12	3	0
1031.5	9	1	2	0	0	0	0	28	0	0	0	0	1	1	0	5	6	0
1039.5	2	1	0	0	0	0	0	23	0	1	0	0	0	0	0	2	11	0
1047.5	4	2	0	0	0	0	0	20	0	0	0	0	1	0	0	1	5	0
1055.5	3	0	0	0	0	0	0	18	0	0	0	0	0	0	0	5	7	0
1063.5	2	1	0	0	0	0	0	8	0	0	0	0	0	0	0	7	5	0
1071.5	6	2	0	0	0	0	1	12	0	0	0	0	0	2	0	10	5	0
1079.5	0	1	1	0	0	0	2	32	0	0	0	0	0	0	0	0	7	0
1087.5	4	2	0	0	0	0	0	5	0	0	0	0	0	0	0	4	3	0
1095.5	5	1	0	0	0	0	1	1	0	0	0	0	0	1	0	6	7	0
1099.5	1	1	3	0	0	0	0	18	0	0	0	1	0	1	0	1	5	0
1103.5	3	1	4	0	2	0	0	27	0	0	0	0	0	1	0	2	2	0
1108.5	4	4	2	0	1	0	0	30	0	0	0	0	0	1	0	2	3	0
1124.5	1	0	9	0	0	0	1	10	0	0	0	1	0	0	0	1	4	0
1127.5	4	4	7	0	0	0	1	8	0	0	0	0	0	0	0	1	5	0
1131.5	0	2	1	0	0	0	0	6	0	0	0	0	0	0	0	1	5	0
1135.5	0	2	0	0	0	0	1	6	0	0	0	0	0	0	0	3	0	0
1139.5	0	10	1	0	0	0	0	5	0	0	0	0	0	0	0	0	0	0
1143.5	2	8	2	0	0	0	0	12	0	0	0	0	0	0	0	0	1	0
1147.5	0	6	3	0	0	0	2	2	0	0	0	0	0	0	0	0	3	0
1151.5	0	0	0	0	0	0	0	0	0	0	0	0	0	0	0	2	1	0
1155.5	0	2	4	0	0	0	0	1	0	0	0	0	0	0	0	0	2	0
1159.5	0	4	1	0	0	0	0	0	0	0	0	0	0	0	0	0	1	0
1163.5	0	2	0	0	0	0	0	0	0	0	0	0	0	0	0	1	3	0
1167.5	0	2	0	0	0	0	0	0	0	0	0	0	0	0	0	1	1	0

Depth (cm)	<i>Cyperus</i>	<i>Dryas</i>	Elaeagnaceae	<i>Ephedra</i>	<i>Eupatorium</i>	Fagaceae	<i>Fagus</i>	<i>Fraxinus</i> <i>americana</i>	<i>Fraxinus</i> <i>pennsylvanica</i>	<i>Fraxinus nigra</i>	<i>Galium</i>	Haloragaceae	<i>Humulus</i>	Indeterminabl e	<i>Iva</i>
903.5	1	0	0	0	0	2	0	0	0	3	2	0	0	6	3
911.5	1	0	0	0	0	0	0	0	1	4	4	2	0	8	4
919.5	0	0	0	0	0	1	0	0	0	3	6	1	0	3	0
927.5	0	0	0	0	0	0	0	0	0	6	2	1	0	3	0
935.5	0	0	0	0	0	2	0	0	0	6	5	1	0	8	0
943.5	0	0	0	0	0	0	0	0	0	4	1	0	0	8	0
951.5	0	0	0	0	0	0	0	0	0	3	2	0	0	5	0
959.5	0	0	0	0	0	0	0	0	0	11	0	0	0	5	0
967.5	1	0	0	0	0	0	0	0	0	5	0	1	0	3	0
975.5	0	0	0	0	0	0	0	0	0	17	1	1	0	5	0
982.5	0	0	0	0	0	0	0	0	0	6	2	0	0	13	7
991.5	0	0	0	2	0	1	0	0	0	19	1	0	0	8	0
999.5	2	0	0	0	0	0	0	0	0	6	3	1	0	4	0
1007.5	0	0	0	0	0	0	0	0	1	7	3	0	0	4	0
1015.5	0	0	0	0	0	0	0	0	0	15	3	1	2	4	1
1023.5	0	0	0	0	0	0	0	0	0	11	4	0	1	5	0
1031.5	0	0	0	0	0	0	0	0	0	13	2	0	0	5	0
1039.5	0	0	0	0	0	0	1	0	1	6	1	2	0	3	0
1047.5	0	0	0	0	0	0	0	0	0	4	2	0	0	8	5
1055.5	0	0	0	0	0	0	1	0	1	10	6	2	0	3	0
1063.5	1	0	0	0	0	0	0	0	1	11	2	0	0	3	0
1071.5	2	0	0	0	0	0	0	0	3	4	2	0	0	1	0
1079.5	0	0	0	0	0	0	1	0	0	6	4	0	0	8	3
1087.5	0	0	0	0	0	0	1	0	0	16	3	1	0	5	0
1095.5	0	0	0	0	0	0	3	0	1	9	1	0	0	7	1
1099.5	0	0	0	0	0	0	0	0	0	5	2	0	0	0	0
1103.5	0	0	0	0	0	0	0	0	0	4	1	1	0	8	3
1108.5	0	0	0	0	0	0	0	0	0	1	1	2	0	8	3
1124.5	0	1	0	0	0	0	0	0	1	14	2	0	0	9	1
1127.5	0	2	0	0	0	0	0	0	0	6	0	0	0	7	4
1131.5	0	0	0	0	0	0	1	0	0	1	0	0	0	6	0
1135.5	0	0	0	0	0	0	0	0	0	9	1	0	0	8	0
1139.5	0	0	0	0	0	0	0	0	0	9	1	0	0	1	1
1143.5	0	0	0	0	0	0	0	0	0	6	1	0	0	13	0
1147.5	0	0	0	0	0	0	0	0	0	4	0	1	0	3	1
1151.5	0	0	0	0	0	0	0	0	0	2	0	0	0	1	0
1155.5	0	0	0	0	0	0	0	0	0	2	0	0	0	0	1
1159.5	0	2	0	0	0	0	0	0	0	1	1	0	0	7	0
1163.5	0	0	0	0	0	0	0	0	1	3	1	1	0	2	0
1167.5	0	0	0	0	0	0	0	0	1	3	1	0	0	4	0

1171.5	0	58	0	1	0	11	141	0	0	2	0	0	0	2	0
1175.5	0	76	0	0	0	2	19	0	0	3	1	0	0	0	0
1179.5	0	73	0	0	0	1	27	0	0	7	0	1	4	1	0
1183.5	7	76	0	0	4	22	30	0	0	2	1	0	0	0	0
1187.5	0	80	0	0	0	0	6	0	0	10	0	0	1	0	0
1191.5	1	95	0	0	0	0	5	0	0	3	0	0	0	0	0
1194.5	0	85	0	0	0	0	3	0	0	7	0	0	4	1	0
1199.5	14	117	0	0	1	0	5	0	0	3	0	0	0	0	0
1203.5	0	111	2	0	0	0	2	0	0	6	0	1	0	0	0
1207.5	0	110	0	0	0	0	5	0	0	4	1	0	1	0	0
1211.5	0	96	0	0	0	0	2	0	0	8	0	0	1	0	0
1215.5	0	173	0	0	0	0	4	0	0	9	0	1	1	0	0
1219.5	0	148	0	0	0	0	6	0	0	2	0	0	0	0	0
1223.5	11	139	0	0	0	0	4	0	0	2	0	0	0	0	0
1231.5	7	203	0	1	4	10	6	0	0	3	0	0	0	0	0
1234.5	0	260	0	0	0	0	12	0	0	3	0	1	0	0	0
1239.5	23	228	0	1	0	5	2	0	0	1	0	0	0	0	0
1242.5	1	282	0	0	0	0	8	0	0	1	0	0	1	0	0
1250.5	0	284	0	0	0	0	5	0	0	0	0	0	3	0	0
1258.5	2	294	0	0	0	0	7	0	0	2	0	0	0	0	0
1266.5	0	273	0	0	1	0	15	0	0	0	0	0	0	0	0
1274.5	2	182	0	0	0	0	18	0	0	3	0	0	0	0	0
1282.5	4	149	0	0	0	0	20	0	0	0	0	1	1	0	0
1290.5	7	243	0	0	0	0	33	0	0	0	0	1	0	0	0
1298.5	14	194	0	0	0	0	24	0	0	0	0	0	2	0	0
1306.5	2	267	0	0	5	0	18	0	0	0	0	0	1	0	0
1313.5	2	234	0	0	1	0	25	0	0	0	0	0	1	0	0
1321.5	0	227	0	0	0	0	46	0	0	0	0	0	0	0	0
1329.5	5	140	0	0	1	1	22	0	0	1	0	0	1	0	0
1337.5	4	137	0	0	0	0	32	0	0	0	0	0	0	0	0
1345.5	5	156	0	0	0	1	30	0	0	0	0	0	0	0	0
1352.5	2	147	0	0	0	0	22	0	0	1	0	0	0	0	0
1360.5	0	156	0	0	0	0	21	0	0	0	0	0	1	0	0
1368.5	0	150	0	0	2	0	19	0	0	4	0	0	1	0	0
1376.5	0	160	0	0	0	0	27	0	0	2	0	0	0	0	0

Depth (cm)	<i>Tilia</i>	<i>Triglochin</i>	<i>Tsuga</i>	<i>Typha</i>	<i>Ulmus undiff.</i>	Unknown	<i>Vitis</i>	<i>Xanthium</i>
903.5	0	0	0	0	39	1	0	0
911.5	0	1	0	0	21	1	0	0
919.5	1	0	0	0	25	1	0	0
927.5	5	0	0	0	22	3	0	0
935.5	2	0	0	0	30	2	1	0
943.5	0	0	0	0	24	0	0	0
951.5	3	0	0	0	20	0	0	0
959.5	2	0	0	0	20	0	0	0
967.5	0	0	0	1	23	1	1	0
975.5	3	0	0	0	27	0	0	0
982.5	1	1	0	1	29	2	0	0
991.5	4	0	0	0	20	3	0	0
999.5	0	0	0	0	21	2	1	0
1007.5	0	0	0	0	30	0	0	0
1015.5	0	0	0	0	26	1	0	0
1023.5	3	0	0	1	33	1	2	0
1031.5	3	0	0	0	25	2	1	0
1039.5	3	0	0	0	32	1	0	0
1047.5	0	0	0	0	23	2	0	0
1055.5	0	0	0	0	33	1	0	0
1063.5	0	0	0	0	28	1	0	0
1071.5	0	0	0	0	22	0	0	1
1079.5	0	0	0	0	23	1	0	0
1087.5	0	0	0	0	20	2	0	0
1095.5	1	0	2	0	24	4	0	0
1099.5	2	0	0	2	25	0	0	0
1103.5	0	1	2	1	19	1	0	0
1108.5	2	0	4	0	31	1	0	0
1124.5	1	0	4	1	36	1	0	0
1127.5	0	0	3	0	26	0	0	0
1131.5	0	0	5	1	20	0	0	0
1135.5	0	0	9	0	22	0	0	0
1139.5	0	0	6	0	16	0	0	0
1143.5	0	0	4	0	20	4	0	0
1147.5	0	0	5	2	16	0	0	0
1151.5	0	0	3	0	10	0	0	0
1155.5	0	0	3	0	8	0	0	0
1159.5	0	0	2	1	13	1	0	0
1163.5	0	0	3	1	7	0	0	0
1167.5	0	0	2	1	8	1	0	0

1171.5	0	0	3	1	11	2	0	0
1175.5	0	1	0	8	14	3	0	0
1179.5	0	0	2	2	16	1	1	0
1183.5	1	1	1	5	19	3	0	0
1187.5	0	0	0	1	14	2	0	0
1191.5	1	1	1	0	15	4	0	0
1194.5	0	2	0	0	10	1	0	0
1199.5	0	0	0	6	7	0	0	0
1203.5	0	0	1	6	11	2	0	0
1207.5	1	0	0	5	14	2	0	0
1211.5	0	0	0	5	7	0	0	0
1215.5	0	0	0	5	2	2	0	0
1219.5	1	1	0	3	5	1	0	0
1223.5	0	0	1	0	6	0	0	0
1231.5	0	0	0	0	3	0	0	0
1234.5	0	0	0	0	0	0	0	0
1239.5	0	0	0	0	1	1	0	0
1242.5	0	0	0	0	0	1	0	0
1250.5	0	0	0	0	0	0	0	0
1258.5	0	0	0	0	0	0	0	0
1266.5	0	0	0	0	0	0	0	0
1274.5	0	0	0	0	0	1	0	0
1282.5	0	0	0	0	0	1	0	0
1290.5	0	0	0	0	0	0	0	0
1298.5	0	0	0	0	1	1	0	0
1306.5	0	0	0	0	0	0	0	0
1313.5	0	0	0	0	0	0	0	0
1321.5	0	0	0	0	0	0	0	0
1329.5	0	0	0	0	0	1	0	0
1337.5	0	0	0	0	0	0	0	0
1345.5	0	0	0	0	0	1	0	0
1352.5	1	0	0	0	0	0	0	0
1360.5	0	0	0	0	0	1	0	0
1368.5	0	0	0	0	0	0	0	0
1376.5	0	0	0	0	0	1	0	0